



# A phase field-based systematic multiscale topology optimization method for porous structures design

Qian Yu, Qing Xia, Yibao Li\*

School of Mathematics and Statistics, Xi'an Jiaotong University, Xi'an 710049, China



## ARTICLE INFO

### Article history:

Received 17 November 2021  
 Received in revised form 19 April 2022  
 Accepted 8 June 2022  
 Available online 23 June 2022

### Keywords:

Porous structures  
 Multiscale topology optimization  
 Phase field method  
 Connectivity  
 Allen-Cahn equation

## ABSTRACT

In this paper, we propose a novel and systematic phase field-based multiscale topology optimization method for porous structures design. The multi-regional microstructural composite and fixed microstructural shapes are adopted to balance the objective and other constraints. The connectivity issue between different microstructures is handled. In the multiscale topology optimization, the macro and micro design variables are updated by the Allen-Cahn type equations which include a reaction-diffusion term, a sensitivity analysis term, a volume constraint term, and a correction term. The correction term is used to keep topologies of macro and micro structures closed to the prescribed structures. We use an efficient merging algorithm to handle the connectivity issue between different microstructures. Based on an interpolation technique of the phase field function and a modified Allen-Cahn equation, this algorithm can smooth the connecting boundaries and satisfy the minimum surface theorem. The final distribution of microstructures keeps the extraordinary physical and mechanical properties for the macrostructure. Some typical cantilever beam, Michell-type structure and Messerschmitt-Bölkow-Blohm beam are performed to verify the effectiveness of our method.

© 2022 Elsevier Inc. All rights reserved.

## 1. Introduction

Porous structures appear widely in nature such as wood, coral, cork, and sponge, etc. The character in common is that they are composed of porous solids with periodically or stochastically distributed cells which results in their low densities. These representative cells are called microstructures which are made from ordinary materials [1]. Inspired by the macrostructures with lightweight but superior structural properties, man-made porous structures were widely studied. Recently, artificially designed porous structures are characterized with superior mechanical properties, e.g. high thermal insulation [2], great liquid absorption [3], superb strength and stiffness [4]. The extraordinary physical and mechanical properties for cellular structures mainly depend on the geometry of their microstructures rather than their material constituents [5]. Therefore multiscale topology optimization, simultaneously considering the design of microstructures being affected by the macrostructural loads and boundary conditions to achieve advantage properties of the composite structure, is greatly important in the field of engineering applications.

Multiscale topology optimization has been widely applied to the minimum compliance problem [6–8], the optimum thermal conductive configurations [9], functionally graded material design [10,11] and frequency responses of cellular com-

\* Corresponding author.

E-mail address: yibaoli@xjtu.edu.cn (Y. Li).

URL: <http://gr.xjtu.edu.cn/web/yibaoli> (Y. Li).

posites [12,13]. The main challenge existing for the multiscale topological design is the choice of topology optimization methods. In the past several decades, topology optimization methods have been mainly classified into the element-based method and the boundary variation method [14,15]. The homogenization method, Solid Isotropic Material with Penalization (SIMP) and Evolutionary Structural Optimization (ESO) are the classical element-based methods. Level set method (LSM) and phase field method (PFM) are two representative boundary variation methods in which implicit functions are introduced to depict topological boundary. The details of these methods are reviewed in next section. Recently, the hybrid approaches become popular to improve the computation efficiency in multiscale topology optimization, e.g. PLSM (Parameterized Level Set Method) combined with the numerical homogenization method [6,7], the homogenization method combined with SIMP [8,12] and two element-based methods combined with PLSM [5,16].

Next important issue we should pay attention to is whether the results obtained by multiscale topology optimization are better than those by the traditional single-scale topology optimization. Long et al. [12] investigated composite macrostructures being composed of identical composite microstructures with their constituent phases having significantly different Poisson's ratios. They used the homogenization method both in macro and micro optimizations. They concluded that the two-scale concurrent design could provide higher frequency responses comparing to those obtained from topology optimizations with exclusive material. Sivapuram et al. [17] verified the multiscale topology optimization has a significant advantage than the single-scale optimization in the design of compliant mechanism. However, they found that in the compliance problem, the optimal design was the single-scale topology optimization of the macrostructure. Similar conclusion could be made in [8]. Although multiscale topology optimization with only one porous microstructure has poor performance in the structural compliance than the single topology optimization, Gao et al. [7] and Wang et al. [18] demonstrated that the multi-regional distribution of multiple microstructures had a notable effect on the improvement of the structural dynamic performance than the configuration of only one identical microstructure.

Another important issue for the multiscale topology optimization is the connectivity of adjacent microstructures. The kinematical connective constraint in [7,18,19] is a common technique to deal with the connectivity. But this technique is always limited by the shape of microstructures which must have solid materials close to the corners or the boundaries. This limitation may have effect on the specially functional materials design. Du [20] introduced a new measure, connectivity index (CI), to quantify the topological connectivity which was added as a constraint into the multiscale topology optimization. The upper bounds of CI could quantitatively control the connectivity. Zhang et al. [13] proposed a sensitivity filtering scheme in a progressive optimization scheme. They found this method could well maintain the interconnections of adjacent prototype microstructures. However, no matter whatever the connected method is, the connectivity of microstructures are always achieved at the cost of stiffness decrease. Wang et al. [18] pointed that it was a common problem in multiscale topology optimization of multiple microstructures. No matter in hybrid approaches such as SIMP in micro-scale optimization combined with the velocity field level set in macro-scale or SIMP method in the macro-scale and micro-scale optimization, the same issue can be encountered.

In this paper, a systematic and efficient phase field-based multiscale topology optimization method is proposed. This is the first work in which the whole framework of multiscale topology optimization is based on phase field method. In the proposed method, focusing on reducing computation time for the topology optimization of composite structure at high resolution and improving the structural performance, we adopt multi-regional microstructure composites design method to balance the objective and various other constraints. The proposed method also assures of fixed microstructures in each subregion. The micro units we choose here are with periodic minimal surfaces. Another highlight is that we propose an interpolation technique to deal with the connectivity between multiple microstructures. The technique consists of two procedures, a merging algorithm and a smooth algorithm. The smooth algorithm is used to assure of microstructures' minimal surface. We will compare the performance of our method with others, including the classical SIMP, the single-scale topology optimization and the multiscale topology optimization with one identical microstructure. The typical cantilever beam, Messerschmitt-Bölkow-Blohm (MBB) beam and Michell-type structures will be performed to verify the utilization of our method.

We organize this paper as follows. In section 2, we review some topology optimization methods and point out the special characters of PFM-based topology optimization. We describe detailedly phase field method for the design of composite structure in section 3. In section 4, we develop a systematic multiscale topology optimization framework with multiple microstructures in the macrostructure. In section 5, numerical schemes for the evolved equations of two-scale design variables are proposed. In section 6, numerical tests are performed to verify our method's convergence, efficiency and practicability. Some concluding remarks are given in Section 7.

## 2. Review of topology optimization methods

The homogenization method and SIMP are firstly proposed to overcome ill-posedness of the original topology optimization [21]. In homogenization method [22,23], the property of macrostructure can be expressed equivalently by isotropic or anisotropic porous microstructures, which greatly reduces the computation complexity of optimizing macrostructures. Then how to determinate and evaluate the size of microstructure and the length ratio between macros and micros become challenging. Although some lattice materials [24] have been built by homogenization method, choosing a length scale is the trickiest part of the whole process. And indeterminate pores in the materials result in difficulties in manufacturing.

SIMP [25] introduces an interpolation between the density design variable and the material property to generate a well-posed optimization problem. But the element-based topology optimization always results in the structural boundary with zigzag and the numerical instability. Generally, additional algorithm such as filter scheme [26], is used to avoid such instability. The disadvantages of the filter scheme are partly that a grey zone of width  $r_{min}$  between solid and void regions is left and partly that it works best for active volume constraints [14]. Another element-based method is ESO [27] or BESO (Bi-directional Evolutionary Structural Optimization) [28] which appears more simple in numerical implementation than SIMP. The basic idea is to gradually remove redundant elements or add efficient elements to achieve an optimal design. This method always focuses on local consequences rather than on the global optimum which is typically computationally expensive.

LSM implicitly tracks structural boundary by the zero isosurface of high-dimensional level set function. For the traditional LSM [29] based on Hamilton–Jacobi partial differential equation (H-J PDE), the procedures of re-initialization and velocity extension are necessary which often cause slow convergence and local minimum. Later the parametric level set method (PLSM) become popular. The core idea of PLSM is to interpolate the original level set function by some radial basis functions (RBF) such that the space and time schemes are separated. PLSM does not need re-initialization and velocity extension anymore, and some well-established structural optimization algorithms, i.e. the optimality criteria (OC), can be used directly. However, it's reported [5,30] that in the compactly supported radial basis functions (CSRBF), the lower accuracy in the numerical interpolation may occur especially when the design of microstructure is subject to a relatively small volume constraint. And it is possible that the optimization process runs into local minima if an initialization is too far from a global minimum. In the globally supported radial basis functions (GSRBF), the full interpolation matrix has great effects on computational efficiency.

PFM has been widely studied in many fields, e.g. thermodynamical systems [31], thin film growth model [32], gradient flow models [33,34]. It is originally used to describe the phase transition in alloy along with the system's energy dissipation which is an essential issue in phase field theory. The interface with a thickness between the phases is introduced. During phase transformation, some phases precipitate in some areas and change into another phase, which leads to the interface complex topologies. From this process point of view, structural topology optimization is a similar problem as phase transition [35,36]. Like LSM, PFM can implicitly track the complex boundaries. The thermodynamic model for topology optimization based on PFM is defined by a variational approach combining with Allen-Cahn (AC) theory [37], considering the bulk energy and interface energy of the phases and the elastic strain energy of the structure. Thus the structural optimization problem is transformed into a phase transition problem defined by a set of nonlinear parabolic PDEs. Although the mass conservation is not assured in AC, a correction term can be added to make the mass conservative [38]. Recently PFM has gradually become popular in the graded material [39,40] because of the introduced wide interface. These promising characteristics of PFM make us further investigate the PFM-based multiscale topology optimization which is never reported according to the author's knowledge.

In this work, we use PFM combining with the homogenization method to optimize structural compliance problems. We first construct an energy including a free energy, structural elastic potential energy, a volume constraint term and a correction term which is used to fix the topologies of macrostructure and microstructures. The evolved equation of design variables, i.e. AC type equation, can be obtained by a variational approach. We use Adam's scheme to discretize in time and finite difference method to discretize in space. This model overcomes the difficulty of indeterminate pores in the materials and doesn't require additional algorithms to avoid the instability. The velocity extension and re-initialization procedures are not required. Besides, the structural boundaries are strongly smooth because of the intrinsic quality of Allen-Cahn type equation. Just like phase transition, nucleating new holes inside the material domain is allowed. By numerical simulations, we verify that the proposed scheme is second order accuracy in both time and space. A large time step in our scheme is allowed so that a large number of iterations is not required. The proposed method has a significant advantage in computation than other methods which will be compared in numerical tests. The independence of the initial designs will be also indicated in these tests.

### 3. Phase field method for multi-scale topology optimization

In this section, we will model the single-scale and the multi-scale topology optimization based on PFM respectively. We use the global coordinate system  $\mathbf{x}$  to depict the position of macrostructure and the local coordinate system  $\mathbf{y}$  to depict the position of microstructure. The superscript  $M$  indicates the macro-scale quantities, and the superscript  $m$  is related to the micro-scale quantities.

#### 3.1. Phase field-based topology optimization for single scale

We use  $\Theta^M$ ,  $\Gamma^M$  and  $\Omega^M$  to denote the macro solid domain, structural boundaries and the reference domain of the macrostructure respectively. The macro void domain can be described as  $\Omega^M/\Theta^M$ . The phase field function ranged from 0 to 1 to determine the mass concentration of material for the macrostructure is introduced:

$$\begin{cases} \phi^M(\mathbf{x}) = 0, & \mathbf{x} \in \Omega^M / \Theta^M, \\ 0 < \phi^M(\mathbf{x}) < 1, & \mathbf{x} \in \Gamma^M \cap \Omega^M, \\ \phi^M(\mathbf{x}) = 1. & \mathbf{x} \in \Theta^M. \end{cases} \tag{1}$$

The linear elasticity equations over  $\Omega^M$  can be written as follows:

$$\begin{cases} \nabla \cdot \sigma(\phi^M, \mathbf{u}^M) = 0, \\ \varepsilon(\mathbf{u}^M) = \frac{1}{2}(\nabla \mathbf{u}^M + (\nabla \mathbf{u}^M)^T), \\ \sigma(\phi^M, \mathbf{u}^M) = \mathbf{D}^M(\phi^M) : \varepsilon(\mathbf{u}^M). \end{cases} \tag{2}$$

Here,  $\mathbf{u}^M$  represents the displacement vector. Let  $\mathbf{D}^M(\phi^M) = (\phi^M)^3 \mathbf{D}$  and  $\mathbf{D}$  is the fourth-order stiffness tensor which can be written as  $D_{ijkl} = 2G(\delta_{ik}\delta_{jl} + \frac{\nu}{1-2\nu}\delta_{ij}\delta_{kl})$ .  $G = \frac{E}{2(1+\nu)}$  represents the shear modulus,  $E$  represents the elasticity modulus,  $\nu$  represents the Poisson's ratio,  $\delta$  represents Dirichlet function.  $\mathbf{A} : \mathbf{B} = \mathbf{A}_{ij}\mathbf{B}_{ij}$  is the inner product of two second-order tensors (summation over repeated indices is implied).

Taking an example of the compliance minimization problem in cantilever beam, assume that  $\Gamma_1^M$  and  $\Gamma_2^M$  are two disjoint boundaries of  $\Omega^M$  and  $(\Gamma_1^M \cup \Gamma_2^M) \subset (\Gamma^M \cap \Omega^M)$ . Let  $\mathbf{u} = \mathbf{0}$  on  $\Gamma_1^M$ . And a traction force  $\mathbf{s}$  is applied on  $\Gamma_2^M$ . The structural optimization objective can be represented as:

$$J(\phi^M) = \int_{\Omega^M} W^M(\phi^M) d\mathbf{x} = \int_{\Omega^M} \frac{1}{2} \varepsilon(\mathbf{u}^M) : \mathbf{D}^M(\phi^M) : \varepsilon(\mathbf{u}^M) d\mathbf{x}, \tag{3}$$

with the volume constraint  $\int_{\Omega^M} \phi^M = V_0^M$  where  $V_0^M$  is the maximum volume fraction of the macrostructure. By taking the variation approach [35,41], we reconstruct a structural energy function to transform Eq. (3) into:

$$J^*(\phi^M) = \eta^M \int_{\Omega^M} W^M(\phi^M) d\mathbf{x} + \int_{\Omega^M} \left( F(\phi^M) + \frac{(\epsilon^M)^2}{2} |\nabla \phi^M|^2 \right) d\mathbf{x} + \frac{\beta^M}{2} \left( A(\phi^M) - V_0^M \right)^2, \tag{4}$$

where the double well potential  $F(\phi^M) = \frac{1}{4}(\phi^M)^2(1 - \phi^M)^2$  and  $|\nabla \phi^M|^2$  are used to penalize the intermediate densities  $\phi^M \in (0, 1)$  and the perimeter respectively. Let  $A(\phi^M) = \int_{\Omega^M} \phi^M d\mathbf{x}$  and the term  $\left( A(\phi^M) - V_0^M \right)^2$  is a volume penalty term.  $\eta^M$  represents a Lagrangian multiplier.  $\epsilon^M$  represents diffusive interface thickness.  $\beta^M$  represent positive penalty factors. Assumed that  $\phi^M$  evolves with the pseudo-time  $t$ ,  $\frac{\partial \phi^M}{\partial t}$  is proportional to the negative gradient of the energy function (4) related to  $\phi^M$ . Thus the structural optimization problem is transformed into the following Allen-Cahn type equation:

$$\frac{\partial \phi^M}{\partial t} = -\eta^M \frac{\partial W^M}{\partial \phi^M} - F'(\phi^M) + (\epsilon^M)^2 \Delta \phi^M - \beta^M \left( A(\phi^M) - V_0^M \right). \tag{5}$$

Eq. (5) consists of four parts, a topology sensitivity term, a reaction-diffusion term and a volume constraint term. And the corresponding energy (4) satisfies the law of dissipation. The interested reader can refer to our previous work in [41] for the proof. The corresponding boundary conditions of Eq. (5) are:

$$\begin{cases} \mathbf{u}^M = \mathbf{0} & \text{on } \Gamma_1^M, \\ \mathbf{n} \cdot \sigma(\phi^M, \mathbf{u}^M) = \mathbf{s} & \text{on } \Gamma_2^M, \\ \mathbf{n} \cdot \sigma(\phi^M, \mathbf{u}^M) = \mathbf{0} & \text{on } \partial \Omega^M / (\Gamma_1^M \cup \Gamma_2^M), \\ \mathbf{n} \cdot \phi^M = 0 & \text{on } \partial \Omega^M. \end{cases} \tag{6}$$

### 3.2. Phase field-based topology optimization for two scales

In this section, we assume that the macrostructure contains several kinds of microstructures and each of them is periodically distributed in different regions of the macrostructure. Here  $\Theta_\tau^m$ ,  $\Gamma_\tau^m$  and  $\Omega_\tau^m$  are used to denote the solid domain, the structural boundaries and the reference domain of the  $\tau$ th microstructure. The macro reference domain  $\Omega^M$  is partitioned into a number of  $\Pi$  micro reference subdomains  $\Omega_\tau^m$ ,  $\tau = 1, \dots, \Pi$ . Each  $\Omega_\tau^m$  is composed of only one type of microstructure. The governing function for the  $\tau$ th microstructure is defined as follows:

$$\begin{cases} \phi_\tau^m(\mathbf{y}) = 0, & \mathbf{y} \in \Omega_\tau^m / \Theta_\tau^m, \\ 0 < \phi_\tau^m(\mathbf{y}) < 1, & \mathbf{y} \in \Gamma_\tau^m \cap \Omega_\tau^m, \quad (\tau = 1, 2, \dots, \Pi) \\ \phi_\tau^m(\mathbf{y}) = 1. & \mathbf{y} \in \Theta_\tau^m \end{cases} \tag{7}$$

**Table 1**  
The criteria of domain partition.

0	0.4	0.6	0.8	1
$0 \leq \phi^M \leq 0.25$	$0.25 < \phi^M \leq 0.5$	$0.5 < \phi^M \leq 0.7$	$0.7 < \phi^M \leq 0.9$	$0.9 < \phi^M \leq 1$

The difference of the evolved equations between two-scale topology optimization and only macro topology optimization is that Eq. (8) includes a correction term which indicates that the resulted solutions get closed to the fixed one as much as possible. Besides, the stiffness tensor  $\mathbf{D}^M$  for the macrostructure is no longer  $(\phi^M)^3\mathbf{D}$  but can be obtained by the homogenization method. We will specify the two difference in next section. The evolved equations for the design variables at macro- and micro-scale can be respectively written as:

$$\begin{cases} \frac{\partial \phi^M}{\partial t} = -F'(\phi^M) + (\epsilon^M)^2 \Delta \phi^M - \eta^M \frac{\partial W^M}{\partial \phi^M} - \gamma^M (\phi^M - \psi^M) - \beta^M (A(\phi^M) - V_0^M), \\ \frac{\partial \phi_\tau^m}{\partial t} = F'(\phi_\tau^m) + (\epsilon_\tau^m)^2 \Delta \phi_\tau^m - \eta_\tau^m \frac{\partial W^M}{\partial \phi^m} - \gamma_\tau^m (\phi_\tau^m - \psi_\tau^m) - \beta_\tau^m (A(\phi_\tau^m) - V_\tau^m), \end{cases} \quad (8)$$

where  $\tau = 1, 2, \dots, \Pi$ . The formulation of terms  $\frac{\partial W^M}{\partial \phi^M}$  and  $\frac{\partial W^M}{\partial \phi^m}$  will be specified in next section.  $V_\tau^m$  is the maximum volume fraction for  $\tau$ th microstructure. The other parameters at micro scale are similar as Eq. (5) which are not explained here.

#### 4. Framework of the multiscale topology optimization for cellular structures design

The whole procedures for the multiscale topology optimization involve three stages: (1) The macro-scale topology optimization is performed to obtain a fixed topology shape of macrostructure; (2) The two-scale concurrent topology optimization is performed to achieve the design of microstructures in the optimal macrostructure; (3) Handling the connectivity between multiple microstructures is performed to successfully transfer macro loads to the whole composite structure. In this section, we still take the structural mean compliance problem as an example. We refer the interested readers to [36] for other problems.

##### 4.1. Macroscale topology optimization

We discretize the macro reference design domain  $\Omega^M$  by  $N$  elements. Let  $\phi_i^M$  represent the design variable of  $i$ th element,  $i = 1, \dots, N$ . The aim of the macro-scale topology optimization problem is to find the optimal distribution of  $\phi_i^M$  to achieve the minimum of  $J^*$ .  $\phi^M$  is evolved by Eq. (5) and the optimal solution can be taken as the fixed topology shape of macrostructure in next stage, which means that  $\psi^M$  in (8) equals the optimal distribution of  $\phi^M$  in the stage of the macro-scale topology optimization.

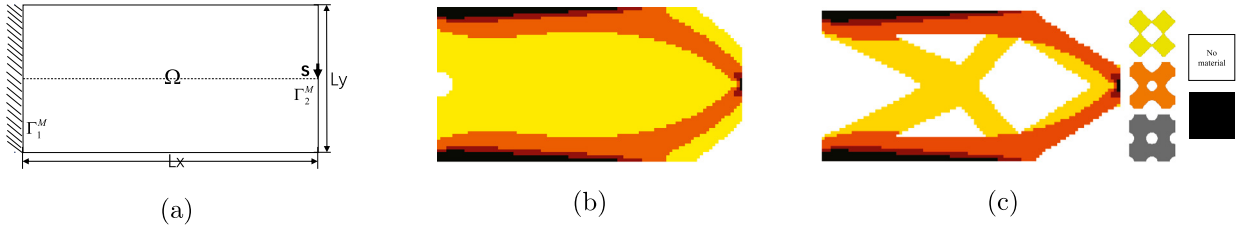
In the first stage, we will partition the macro reference domain  $\Omega^M$  into the number of  $\Pi$  micro reference subdomains  $\Omega_\tau$  ( $\tau = 1, \dots, \Pi$ ). The design variables with the same or proximal densities will be classified into the same subdomain (see the example in Table 1). The macro reference domain  $\Omega^M$  is approximately partitioned into five subdomains. Then we use the following regularized mechanism [6,7] to obtain the regularized density in each subdomain. As shown in Fig. 1(b), different colors represent different regularized density domains.

$$\bar{\phi}^\tau = \frac{1}{N^\tau} \sum_{i=1}^{N^\tau} \phi_{\tau,i}^M \quad (\tau = 1, 2, \dots, \Pi), \quad (9)$$

where  $\phi_{\tau,i}^M$  is the  $i$ th macro element density in the  $\tau$ th subdomain.  $N^\tau$  is the total number of the elements in the  $\tau$ th subdomain, and  $\bar{\phi}^\tau$  is the regularized density of the  $\tau$ th subdomain which is defined by the mean value of all the element densities in this subdomain. The value of  $\bar{\phi}^\tau$  can be used to choose the fixed topology shapes of multiple microstructures by machine learning [42] or other methods, which may equal the porosity or the maximum volume fraction of the  $\tau$ th fixed microstructures. Finally, we use the concurrent topology optimization to fill different subdomains with multiple kinds of microstructures as shown in Fig. 1(c).

##### 4.2. Multiscale concurrent topology optimization

This stage aims to find the optimal topology shapes of distinct microstructures subject to the macro load and boundary conditions. In the previous concurrent optimization [6,13], the computing cost was prohibitive and manufacturing was challenging, because the topology shapes of macrostructure and all types of microstructures might demand optimization. In practical manufacture, remaining the topology of macrostructure can save much computing cost. We will use the multi-scale concurrent topology optimization method to achieve the following properties: (1) the optimal distribution of macro



**Fig. 1.** The schematic diagram of cantilever beam structure (a); the regularized domain (b); the optimal composite macrostructure (c).

and micro design variables for the extraordinary physical and mechanical properties of cellular structures; (2) the topology of macrostructure being maintained; (3) the shapes of microstructures being kept as much as closed to the chosen microstructures.

Next we give a brief description of the conventional mathematical formulations of multiscale concurrent topology optimization. Similarly as the definition of  $\Omega_\tau^m$  in Section 4.1,  $\Omega_\tau^M$  is defined as the macro reference subregion which includes all macro elements belonging to  $\Omega_\tau^m$ . We discretize the micro reference domain  $\Omega_\tau^m$  into the number of  $N_\tau^m$  elements.  $\phi_{\tau,j}^m$ , the micro design variables, represents the density fraction of the  $j$ th element in  $\Omega_\tau^m$ . The objective in multiscale topology optimization is to find the optimal distribution of  $\phi_i^M$  and  $\phi_{\tau,j}^m$  to minimize the compliance of the macrostructure,  $J(\phi^M, \phi^m)$ . The conventional mathematical equation of multiscale concurrent topology optimization is given as:

$$\begin{cases} \text{find: } \phi_i^M, \phi_{\tau,j}^m \quad (i = 1, \dots, N^M; \tau = 1, \dots, \Pi; j = 1, \dots, N_\tau^m) \\ \text{min: } J(\phi^M, \phi_\tau^m) = \sum_{\tau=1}^{\Pi} \int_{\Omega_\tau^M} \frac{1}{2} \varepsilon(\mathbf{u}_\tau^M) : (\phi_\tau^M)^3 \mathbf{D}_\tau^H : \varepsilon(\mathbf{u}_\tau^M) dx. \\ \text{s.t.} \begin{cases} \sum_{\tau=1}^{\Pi} \int_{\Omega_\tau^M} \varepsilon(\mathbf{u}_\tau^M) : (\phi_\tau^M)^3 \mathbf{D}_\tau^H : \varepsilon(\mathbf{v}_\tau^M) dx = \int_{\partial\Omega^M} \mathbf{s} \cdot \mathbf{v}^M ds, \quad \forall \mathbf{v}_\tau^M \in \mathbf{V}(\Omega_\tau^M), \quad \forall \mathbf{v}^M \in \mathbf{V}(\Omega^M) \\ \int_{\Omega_\tau^m} \varepsilon(\mathbf{u}_\tau^m) : (\phi_\tau^m)^3 \mathbf{D}_\tau^m : \varepsilon(\mathbf{v}_\tau^m) dy = \int_{\Omega_\tau^m} \varepsilon(\mathbf{u}_\tau^0) : (\phi_\tau^m)^3 \mathbf{D}_\tau^m : \varepsilon(\mathbf{v}_\tau^m) dy, \quad \forall \mathbf{v}_\tau^m \in \mathbf{V}(\Omega_\tau^m) \\ \mathbf{D}_\tau^H = \frac{1}{|\Theta_\tau^m|} \int_{\Omega_\tau^m} (\varepsilon(\mathbf{u}_\tau^0) - \varepsilon(\mathbf{u}_\tau^m)) : (\phi_\tau^m)^3 \mathbf{D}_\tau^m : (\varepsilon(\mathbf{u}_\tau^0) - \varepsilon(\mathbf{u}_\tau^m)) dy, \\ \int_{\Omega^M} \phi^M dx \leq V_0^M, \quad \int_{\Omega_\tau^m} \phi_\tau^m dy \leq V_\tau^m, \quad V_\tau^m = \bar{\phi}^\tau, \quad \tau = 1, \dots, \Pi. \end{cases} \end{cases} \quad (10)$$

$\mathbf{u}_\tau^M$  represents the displacement vector of all macro elements in the subregion  $\Omega_\tau^M$ .  $\phi_\tau^M$  represents the density of all macro elements in the subregion  $\Omega_\tau^M$ .  $\mathbf{u}_\tau^m$  represents the displacement vector of all micro elements in the subregion  $\Omega_\tau^m$ .  $|\Theta_\tau^m|$  represents the area of  $\Omega_\tau^m$ .  $\mathbf{V}$  is the kinematically admissible displacement space. The homogenized effective stiffness matrices  $\mathbf{D}_\tau^H$  of all the  $\tau$ th representative microstructures are evaluated by the numerical homogenization method [23].  $\mathbf{D}_\tau^m$  represents stiffness tensor of  $\tau$ th microstructure.  $\mathbf{u}_\tau^0$  represents the initial unit test displacement field.  $V_0^M$  represents the prescribed total material consumption.  $V_\tau^m$  represents the volume constraint of the  $\tau$ th microstructure, which equals the regularized density  $\bar{\phi}^\tau$ . The first-order derivatives of the objective function with respect to the macro and micro design variables are expressed as follows:

$$\frac{\partial J}{\partial \phi^M} = \int_{\Omega^M} \frac{\partial W^M}{\partial \phi^M} dx = - \sum_{\tau=1}^{\Pi} \int_{\Omega_\tau^M} \frac{1}{2} \varepsilon(\mathbf{u}_\tau^M) : 3(\phi_\tau^M)^2 \mathbf{D}_\tau^H : \varepsilon(\mathbf{u}_\tau^M) dx. \quad (11)$$

$$\frac{\partial J}{\partial \phi_\tau^m} = \int_{\Omega^M} \frac{\partial W^M}{\partial \phi_\tau^m} dx = - \int_{\Omega_\tau^M} \frac{1}{2} \varepsilon(\mathbf{u}_\tau^M) : (\phi_\tau^M)^3 \frac{\partial \mathbf{D}_\tau^H}{\partial \phi_\tau^m} : \varepsilon(\mathbf{u}_\tau^M) dx. \quad (12)$$

$$\frac{\partial \mathbf{D}_\tau^H}{\partial \phi_\tau^m} = \frac{1}{|\Theta_\tau^m|} \int_{\Omega_\tau^m} (\varepsilon(\mathbf{u}_\tau^0) - \varepsilon(\mathbf{u}_\tau^m)) : 3(\phi_\tau^m)^2 \mathbf{D}_\tau^m : (\varepsilon(\mathbf{u}_\tau^0) - \varepsilon(\mathbf{u}_\tau^m)) dy. \quad (13)$$

Here we reconstruct a new objective function based on phase field method in a similar way with that in Section 3.1.

$$\begin{aligned}
 & find : \phi_i^M, \phi_{\tau,j}^m \quad (i = 1, \dots, N^M; \tau = 1, \dots, \Pi; j = 1, \dots, N_\tau^m) \\
 & \min : J^*(\phi^M, \phi_\tau^m) = \eta^M J(\phi^M, \phi_\tau^m) + \int_{\Omega^M} \left( F(\phi^M) + \frac{(\epsilon^M)^2}{2} |\nabla \phi^M|^2 \right) d\mathbf{x} + \frac{\gamma^M}{2} \int_{\Omega^M} (\phi^M - \psi^M)^2 d\mathbf{x} \\
 & \quad + \frac{\beta^M}{2} \left( A(\phi^M) - V_0^M \right)^2. \\
 & \text{s.t.} \begin{cases} \sum_{\tau=1}^{\Pi} \int_{\Omega_\tau^M} \varepsilon(\mathbf{u}_\tau^M) : (\phi_\tau^M)^3 \mathbf{D}_\tau^H : \varepsilon(\mathbf{v}_\tau^M) d\mathbf{x} = \int_{\partial\Omega^M} \mathbf{s} \cdot \mathbf{v}^M ds, \quad \forall \mathbf{v}_\tau^M \in \mathbf{V}(\Omega_\tau^M), \quad \forall \mathbf{v}^M \in \mathbf{V}(\Omega^M) \\ \int_{\Omega_\tau^m} \varepsilon(\mathbf{u}_\tau^m) : (\phi_\tau^m)^3 \mathbf{D}_\tau^m : \varepsilon(\mathbf{v}_\tau^m) d\mathbf{y} = \int_{\Omega_\tau^m} \varepsilon(\mathbf{u}_\tau^0) : (\phi_\tau^m)^3 \mathbf{D}_\tau^m : \varepsilon(\mathbf{v}_\tau^m) d\mathbf{y}, \quad \forall \mathbf{v}_\tau^m \in \mathbf{V}(\Omega_\tau^m) \\ \mathbf{D}_\tau^H = \frac{1}{|\Theta_\tau^m|} \int_{\Omega_\tau^m} \left( \varepsilon(\mathbf{u}_\tau^0) - \varepsilon(\mathbf{u}_\tau^m) \right) : (\phi_\tau^m)^3 \mathbf{D}_\tau^m : \left( \varepsilon(\mathbf{u}_\tau^0) - \varepsilon(\mathbf{u}_\tau^m) \right) d\mathbf{y}, \\ \int_{\Omega_\tau^m} \phi_\tau^m d\mathbf{y} \leq V_\tau^m, \quad V_\tau^m = \bar{\phi}^\tau, \quad \tau = 1, \dots, \Pi. \end{cases} \tag{14}
 \end{aligned}$$

Here,  $\psi^M$  is used to define the fixed topology shape of macrostructure in  $\Omega^M$ . The correction term  $\int_{\Omega^M} (\phi^M - \psi^M)^2 d\mathbf{x}$  makes solution  $\phi^M$  close to the fixed shapes  $\psi^M$  as much as possible.  $\gamma^M$  is a positive parameter. With two terms  $\frac{\partial W^M}{\partial \phi^M}$  and  $\frac{\partial W^M}{\partial \phi^m}$  obtained from Eqs. (11)-(13),  $\phi^M$  and  $\phi_\tau^m$  can be evolved by Eq. (8).  $\mathbf{D}_\tau^m$  is the fourth-order stiffness tensor, which can be represented as  $D_{\tau,ijkl}^m = 2G_\tau(\delta_{ik}\delta_{jl} + \frac{\nu_\tau}{1-2\nu_\tau}\delta_{ij}\delta_{kl})$ .  $G_\tau$  and  $\nu_\tau$  are the elasticity property of  $\tau$ th microstructure. For simplicity, we assume all microstructures have same material property,  $\mathbf{D} = \mathbf{D}_\tau^m$ ,  $G = G_\tau$ ,  $\nu = \nu_\tau$  ( $\tau = 1, \dots, \Pi$ ).

### 4.3. Connectivity between multiple microstructures

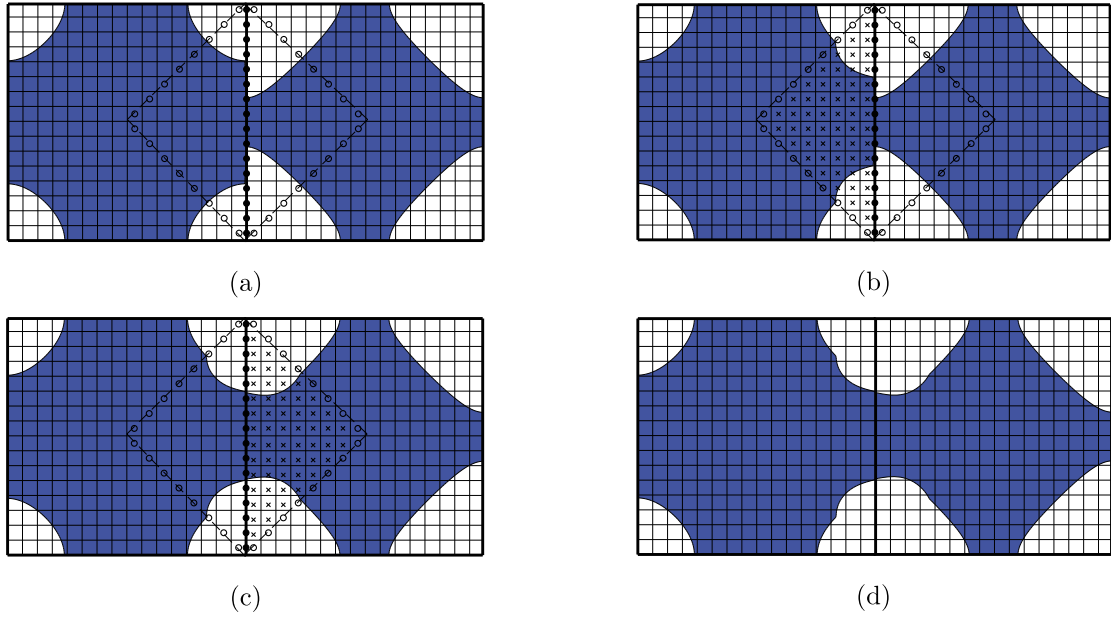
In the stage of multi-scale concurrent topology optimization, the different microstructures in the adjacent regions may not be well connected. Poor micro-structural connectivity makes microstructures unable to transfer loads exactly as expected by the homogenization theory. We will present an efficient method to deal with the connectivity problem. Connectivity techniques involve two steps: (1) connecting the boundaries between multiple microstructures by a merging algorithm; (2) optimizing topologies of the connected microstructures subject to the macro loads and boundary conditions.

For the first step, we refer to our merging algorithm in [43]. This algorithm uses an interpolation technique based on the phase field function to connect different microstructures directly. Taking two periodic cells as an example, the two cells have constant curvatures on their boundaries but different porosities, shown in Fig. 2(a). The goal is to naturally connect the adjoining boundaries. We know circle  $\circ$  on the diagonal lines of the two periodic cells. Filled circle  $\bullet$  is used to represent the average density of overlapping part for the two cells. The point represented by a cross  $\times$  can be interpolated linearly by two ending points  $\circ$  and  $\bullet$  which locate in the same horizontal line with the cross. We firstly perform the interpolation technique for the left cell and obtain the result as Fig. 2(b). Then we perform the interpolation technique for the right cell and obtain the result as Fig. 2(c). Fig. 2(d) show the merged shapes for the two cells after connecting. We use  $\varphi^m$  to define the micro design variable after the interpolation technique in the adjacent regions.

For the second step, because the geometrical symmetry of the micro cells is broken after operations of the first step, the concurrent multiscale topology optimization model (14) is used to ensure that the connection effect is considered in optimization. However, before going that, the connected boundaries will be smoothed to satisfy the property of minimal surfaces [38] which is often used to measure stability of structures. We adapt the following AC type equation (15) to smooth the boundaries between different micro cells. Here,  $\varphi^m$  is used to represent the connected macrostructure obtained by the first step.

$$\begin{aligned}
 \frac{\partial \phi_\tau^m}{\partial t} &= -\frac{F'(\phi_\tau^m)}{(\epsilon_\tau^m)^2} + \Delta \phi_\tau^m - \gamma_\tau^m (\phi_\tau^m - \varphi^m) - \lambda \frac{\phi_\tau^m (1 - \phi_\tau^m)}{\sqrt{2}\epsilon}, \\
 \lambda &= \frac{-\sqrt{2} \int_{\Omega^m} F'(\phi_\tau^m) d\mathbf{y}}{\epsilon \int_{\Omega^m} \phi_\tau^m (1 - \phi_\tau^m) d\mathbf{y}}. \tag{15}
 \end{aligned}$$

The term  $-\lambda \frac{\phi_\tau^m (1 - \phi_\tau^m)}{\sqrt{2}\epsilon}$  in Eq. (15) is used to satisfy  $\varphi^m$  the property of minimal surface.  $\lambda$  is the average value of mean curvature over the surface. Then we perform the concurrent topology optimization in stage 2. It is noted that the operations in the connectivity stage of the proposed framework only affect the micro cells between two adjacent subregions, thus we only need to optimize the relating multiscale design variables using (14) to save computation time. Finally, we can obtain



**Fig. 2.** Schematic of connecting boundaries in the 2D domain by a merging algorithm. (a) The shapes before connecting. (b) Interpolation points represented by  $\times$  according to two ending points represented by  $\circ$  and  $\bullet$  for the left cell. (c) Interpolation points represented by  $\times$  according to two ending points represented by  $\circ$  and  $\bullet$  for the right cell. (d) The shapes after connecting.

the optimal distribution of connected microstructures in the optimized macrostructure which has an excellent mechanical property.

**5. Numerical implementation**

The numerical schemes of Eq. (8) in multiscale concurrent topology optimization will be proposed here. Before going that, some notations need to be stated. We use a uniform mesh to discretize the macro design domain  $\Omega^M$ .  $L_x$  and  $L_y$  are the width and length of  $\Omega^M$ . The length of the macro uniform mesh is  $h^M$ . And  $h^M = L_x/N_x^M = L_y/N_y^M$  is defined. The center of each macro element is located at  $\mathbf{x}_{ij} = (x_i, y_j) = ((i - 0.5)h^M, (j - 0.5)h^M)$  for  $i = 1, \dots, N_x^M$ ;  $j = 1, \dots, N_y^M$ .  $N_x^M$  and  $N_y^M$  are the numbers of macro elements in  $x$ - and  $y$ -directions. Let  $(\phi^M)_{ij}^n$  be approximations of  $\phi^M(x_i, y_j, n\Delta t^M)$ , where  $\Delta t^M = T^M/N_t^M$  is the macro time step,  $T^M$  is the macro final time, and  $N_t^M$  is the macro total number of time steps. Similarly, we discretize a micro element into  $N_x^m \times N_y^m$  mesh with  $h^m = l_x/N_x^m = l_y/N_y^m$ .  $l_x$  and  $l_y$  are the width and length of one micro element. Thus the length-scale between micro and macro is  $\varrho = \frac{l_x}{L_x}$ .  $N_x^m$  and  $N_y^m$  are the numbers of micro elements in  $x$ - and  $y$ - directions. The center of each micro element is located at  $\mathbf{y}_{ij} = (x_i, y_j) = ((i - 0.5)h^m, (j - 0.5)h^m)$  for  $i = 1, \dots, N_x^m$ ;  $j = 1, \dots, N_y^m$ . Let  $(\phi_\tau^m)_{ij}^n$  be approximations of  $\phi_\tau^m(x_i, y_j, n\Delta t_\tau^m)$ , where  $\Delta t_\tau^m = T_\tau^m/N_{t,\tau}^m$  is the time step for  $\tau$ th microstructure,  $T_\tau^m$  is the final time, and  $N_{t,\tau}^m$  is the total number of time steps. Let  $N_\tau^m$  be the total numbers of micro elements in the subregion  $\Omega_\tau$  and the area of  $\Omega_\tau$  is defined as  $|\Omega_\tau|$ . Correspondingly,  $(\phi_{\tau,k}^m)_{ij}^n$  represents  $\phi_\tau^m(x_i, y_j, n\Delta t_\tau^m)$  in the  $k$ th micro element of  $\Omega_\tau$ ,  $k = 1, 2, \dots, N_\tau^m$ . In order to get a second-order accurate numerical scheme, we use the finite difference method and Adam's time discretization method. The numerical schemes of Eq. (8) are given as follows:

$$\frac{3(\phi^M)^{n+1} - 4(\phi^M)^n + (\phi^M)^{n-1}}{2\Delta t^M} = -\tilde{F}'((\phi^M)^{n+1}) - \frac{1}{2}(\tilde{\phi}^M)^{n+1} + \frac{1}{2}(\phi^M)^{n+1} + (\epsilon^M)^2 \Delta_d(\phi^M)^{n+1} - \eta^M(w^M)^n - \gamma^M((\phi^M)^n - \psi^M) - \beta^M(A_d((\phi^M)^n) - V_0^M), \tag{16}$$

$$\frac{3(\phi_\tau^m)^{n+1} - 4(\phi_\tau^m)^n + (\phi_\tau^m)^{n-1}}{2\Delta t^m} = -\tilde{F}'((\phi_\tau^m)^{n+1}) - \frac{1}{2}(\tilde{\phi}_\tau^m)^{n+1} + \frac{1}{2}(\phi_\tau^m)^{n+1} + (\epsilon_\tau^m)^2 \Delta_d(\phi_\tau^m)^{n+1} - \eta_\tau^m(w_\tau^m)^n - \gamma^m((\phi_\tau^m)^n - \psi_\tau^m) - \beta^m(A_d((\phi_\tau^m)^n) - V_\tau^m). \tag{17}$$

In Eq. (16), we have

$$(\tilde{\phi}^M)^{n+1} = 2(\phi^M)^n - (\phi^M)^{n-1}, \quad \tilde{F}'((\phi^M)^{n+1}) = 2F'((\phi^M)^n) - F'((\phi^M)^{n-1}),$$



$$A_d((\phi^M)^n) = (h^M)^2 \sum_{i=1}^{N_x^M} \sum_{j=1}^{N_y^M} (\phi^M)_{ij}^n, \quad (w^M)^n = -\frac{1}{2} \sum_{\tau=1}^{\Pi} \varepsilon((\mathbf{u}_\tau^M)^n) : 3((\phi_\tau^M)^n)^2 \mathbf{D}_\tau^H : \varepsilon((\mathbf{u}_\tau^M)^n).$$

$$\mathbf{D}_\tau^H = \frac{1}{|\Theta_\tau^m|} \sum_{k=1}^{N_\tau^m} \left( \varepsilon((\mathbf{u}_\tau^0)^n) - \varepsilon((\mathbf{u}_\tau^m)^n) \right) : ((\phi_{\tau,k}^m)^n)^3 \mathbf{D}_\tau^m : \left( \varepsilon((\mathbf{u}_\tau^0)^n) - \varepsilon((\mathbf{u}_\tau^m)^n) \right).$$

In Eq. (17), we have

$$(\tilde{\phi}_\tau^m)^{n+1} = 2(\phi_\tau^m)^n - (\phi_\tau^m)^{n-1}, \quad \tilde{F}'((\phi_\tau^m)^{n+1}) = 2F'((\phi_\tau^m)^n) - F'((\phi_\tau^m)^{n-1}),$$

$$A_d((\phi_\tau^m)^n) = (h^m)^2 \sum_{i=1}^{N_x^m} \sum_{j=1}^{N_y^m} (\phi_\tau^m)_{ij}^n, \quad (w_\tau^m)^n = -\frac{1}{2} \varepsilon((\mathbf{u}_\tau^M)^n) : ((\phi_\tau^M)^{n+1})^3 \frac{\partial \mathbf{D}_\tau^H}{\partial (\phi_\tau^m)^n} : \varepsilon((\mathbf{u}_\tau^M)^n),$$

$$\frac{\partial \mathbf{D}_\tau^H}{\partial (\phi_\tau^m)^n} = \frac{1}{|\Theta_\tau^m|} \sum_{k=1}^{N_\tau^m} \left( \varepsilon((\mathbf{u}_\tau^0)^n) - \varepsilon((\mathbf{u}_\tau^m)^n) \right) : 3((\phi_{\tau,k}^m)^n)^2 \mathbf{D}_\tau^m : \left( \varepsilon((\mathbf{u}_\tau^0)^n) - \varepsilon((\mathbf{u}_\tau^m)^n) \right).$$

Let  $(\varphi_{ij}^m)^n$  be approximations of  $\varphi^m(x_i, y_j, n\Delta t)$ .  $\Delta t = T/N_t$  is the time step.  $T$  is the final time, and  $N_t$  is the total number of time steps. The second-order accurate numerical scheme of Eq. (15) is given by:

$$\frac{3(\phi_{ij}^m)^{n+1} - 4(\phi_{ij}^m)^n + (\phi_{ij}^m)^{n-1}}{2\Delta t} = -\frac{\tilde{F}'((\phi_{ij}^m)^{n+1}) - (\tilde{\phi}_{ij}^m)^{n+1}/2 + (\phi_{ij}^m)^{n+1}/2}{\epsilon^2} + \Delta_d(\phi_{ij}^m)^{n+1}$$

$$- \gamma^m \left( (\phi_{ij}^m)^n - (\varphi_{ij}^m)^n \right) - \frac{\lambda^{n+1} (\tilde{\phi}_{ij}^m)^{n+1} (1 - (\tilde{\phi}_{ij}^m)^{n+1})}{\sqrt{2}\epsilon}, \tag{18}$$

$$\lambda^{n+1} = \frac{-\sqrt{2} \sum_{i=1}^{N_x^m} \sum_{j=1}^{N_y^m} \tilde{F}'((\phi_{ij}^m)^{n+1})}{\epsilon \sum_{i=1}^{N_x^m} \sum_{j=1}^{N_y^m} (\tilde{\phi}_{ij}^m)^{n+1} (1 - (\tilde{\phi}_{ij}^m)^{n+1})}.$$

Next we will show the flowchart of our proposed method in Fig. 3. The first stage is to obtain the fixed topology shapes of macrostructure. The regularized density is also required for choosing the appropriate microstructures. The second stage is to optimize the topology shapes of microstructures in the macrostructure subject to the macro loads and boundary conditions. The third stage is to solve the connectivity between multiple microstructures and make sure the distribution of microstructures satisfying the objective of the topology optimization of macrostructure.

### 6. Numerical examples

Some classical mechanical structures are performed to verify the utility of our proposed method. Unless otherwise specified, the material parameters are set as  $E = 1$  and  $\nu = 0.3$ . The other parameters in Eqs. (16)-(18) are chosen as  $\epsilon^M = \epsilon^m = \epsilon = 5/(2\sqrt{2} \tanh^{-1}(0.9))$ ,  $\Delta t^M = \Delta t^m = \Delta t = 0.01$ . The tolerance for the macro design variable is represented as  $\phi_{tol}^M = 0.01$  and for the micro design variable is  $\phi_{tol}^m = 0.001$ .

#### 6.1. Convergence test

Convergence test for the macro and micro design variables in concurrent topology optimization will be performed in this section. For simplicity, one kind of periodic microstructure will be designed in this test. We first verify that the schemes Eqs. (16) and (17) are second order accurate in time and space respectively. The macro computational domain  $\Omega^M = (0, 1) \times (0, 1)$  is respectively discretized with mesh  $16 \times 16, 32 \times 32, 64 \times 64, 128 \times 128, 256 \times 256$ , and the corresponding spatial step sizes  $h^M$  are  $1/16, 1/32, 1/64, 1/128, 1/256$  respectively. The micro cell is discretized in  $32 \times 32$ . When the convergence of macro variables is compared, the volume fraction of micro unit is kept to be all the same. The initial shapes of macro-scale are set as:

$$\phi^M(x, y, 0) = 0.25 \times (2 - \cos(3\pi x) + \cos(3\pi y)). \tag{19}$$

The macro-scale parameters  $\epsilon^M = 0.01, \eta^M = 0.1, \gamma^M = 0.5, \beta^M = 0.5$  are taken. The micro-scale parameters  $\epsilon^m = 0.005, \eta^m = 0.1, \gamma^m = 0.5, \beta^m = 0.5$  are taken. Here Cauchy error [41] will be used since the exact solution is not known. Table 2 shows the accuracy of macro design variable is indeed second order. To test the microscale convergence, we keep the macro computation as  $\Omega_M = (0, 1) \times (0, 1)$  but discretize it with mesh  $8 \times 8$ . Thus the length ratio between the macro and the micro is  $\varrho = 1/8$ . The microstructure is discretized with mesh  $16 \times 16, 32 \times 32, 64 \times 64, 128 \times 128, 256 \times 256$ , and the corresponding spatial step sizes  $h^m$  are  $1/16\varrho, 1/32\varrho, 1/64\varrho, 1/128\varrho, 1/256\varrho$  respectively. The volume fraction of

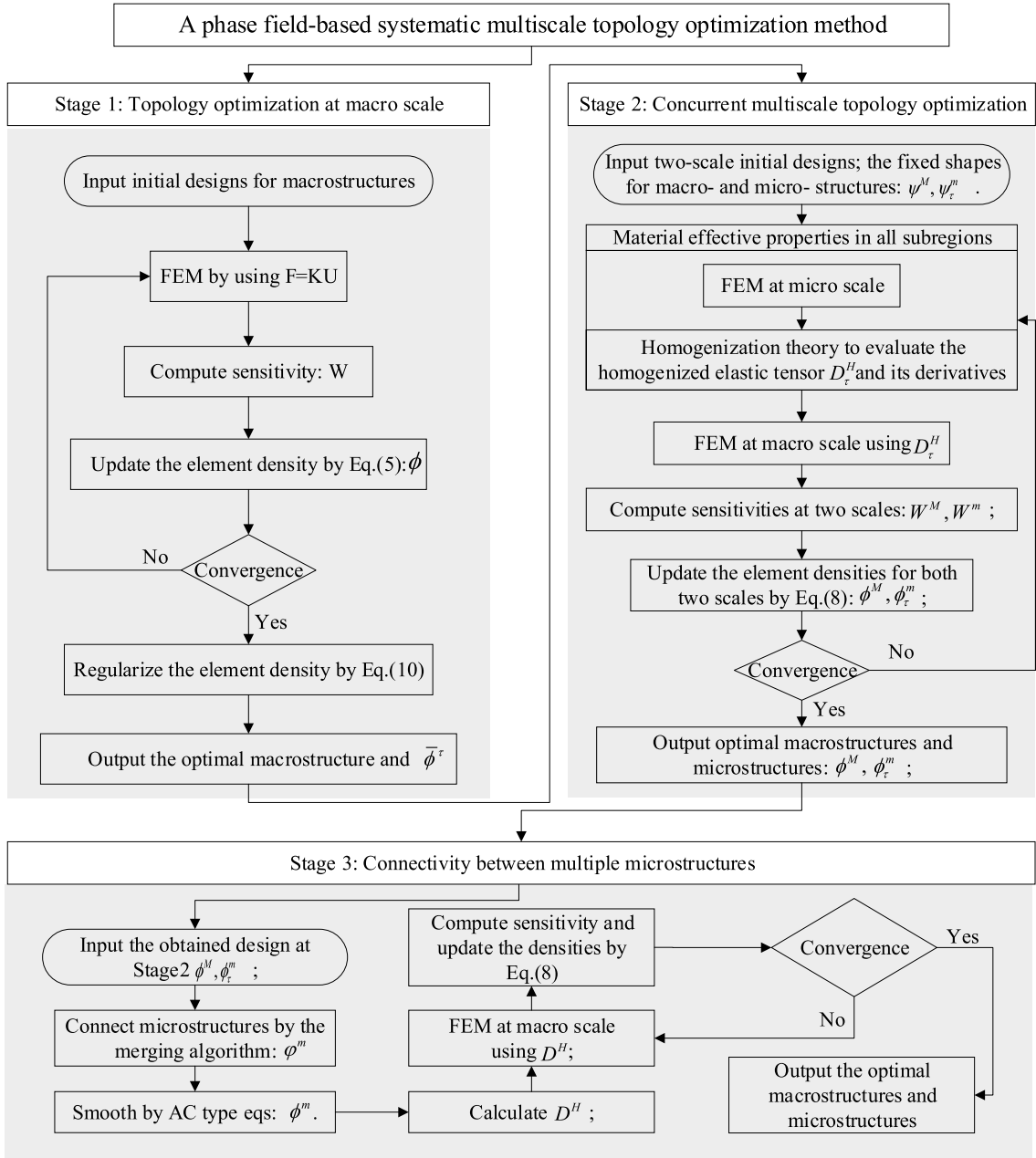


Fig. 3. The flowchart of the proposed systematic multiscale topology optimization method.

macrostructure is assumed to all the same to greatly reduce the impact of macroscale on the microscale. The initial shapes of micro unit are set as same as Eq. (19). We take the parameters as  $\epsilon^m = 1.40, \eta^m = 10, \gamma^m = 5, \beta^m = 10$  in microscale and  $\epsilon^M = 1.50, \eta^M = 1.0, \gamma^M = 5, \beta^M = 5$  in macroscale. The results are shown in Table 3 which are approximate to two, which implies that our method has second-order accuracy in time and space.

### 6.2. Concurrent optimization with a single microstructure

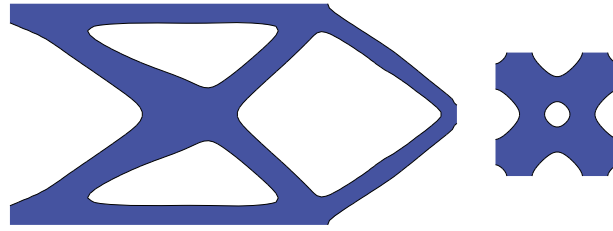
In this section, we will verify the scheme's stability in concurrent topology optimization. Besides, the comparison with SIMP method will be made. For simplicity, here we only consider one microstructure in the macrostructure, thus the connectivity problem does not exist. Taking a cantilever beam as an example, the design schematic is shown as Fig. 1(a). The left side of the beam is fixed and at middle of the right side, a traction force  $\mathbf{s} = -1$  is loaded. Let's assume  $Lx = 2, Ly = 1, N_x^M = 100, N_y^M = 50, h^M = 0.02, lx = 0.02, ly = 0.02, N_x^m = 50, N_y^m = 50$ . We firstly perform the macro topology optimization

**Table 2**  
Error and convergence rates of the macro design variables for the second-order scheme Eq. (16).  $\Delta t = 0.01h^M$  is chosen.

$h_c^M$	$h_f^M$	$\ \phi_{h_c^M} - \phi_{h_f^M}\ _{L_2}$	Rate
$16 \times 16$	$32 \times 32$	$2.400e - 03$	
$32 \times 32$	$64 \times 64$	$5.997e - 04$	1.995
$64 \times 64$	$128 \times 128$	$1.501e - 04$	1.998
$128 \times 128$	$256 \times 256$	$3.754e - 05$	1.999

**Table 3**  
Error and convergence rates of the micro design variables for the second-order scheme Eq. (17).  $\Delta t = 0.01h^m$  is chosen.

$h_c^M$	$h_f^M$	$\ \phi_{h_c^M} - \phi_{h_f^M}\ _{L_2}$	Rate
$16 \times 16$	$32 \times 32$	$7.000e - 03$	
$32 \times 32$	$64 \times 64$	$2.000e - 03$	1.817
$64 \times 64$	$128 \times 128$	$4.9708e - 04$	2.005
$128 \times 128$	$256 \times 256$	$1.3314e - 04$	1.901



**Fig. 4.** The optimal shapes of macrostructure in stage 1 and the fixed shape of the single microstructure in stage 2.

to obtain the optimal topology shape of macrostructure which will remain in the stage of concurrent topology optimization. The optimal topology shape of macrostructure is shown as Fig. 4. In the stage of concurrent topology optimization with one microstructure, we choose a micro unit with P surface as the fixed shape of microstructure shown in Fig. 4. The parameters for the macroscale are:  $V_0^M = 0.4$ ,  $\eta^M = 0.2$ ,  $\beta^M = 2$  and  $\gamma^M = 2$ . The parameters for the microscale are:  $V^m = 0.6$ ,  $\eta^m = 0.1$ ,  $\beta^m = 1$ ,  $\gamma^m = 1$ . The interface thickness is  $\epsilon^M = \epsilon^m = 0.1$ . The initial condition for macroscale is set as  $\phi_0^M = V_0^M$  and for microscale the initial condition is chosen as same as that in Fig. 4(b), i.e.

$$\phi_0^m = 2 \cos 2\pi x \cos 2\pi y - 2(\cos 4\pi x + \cos 4\pi y). \tag{20}$$

In order to verify the stability of the schemes Eqs. (16) and (17), we choose different time steps  $\Delta t = 0.1h^M, h^M$  and  $100h^M$  to evolve the multiscale design variables. The total time is  $T = 300h^M$ . The results are shown in Fig. 5(a)-(c), from which we can see that the large time step is allowed but the optimal designs obtained by the small time steps are more similar with those in Fig. 4. Therefore, to computatively more accurate and more efficient, we prefer an adaptive time step  $\Delta t = h^M 1.05^{iter-1}$  to optimize which is shown in Fig. 5(d).

Next, we will compare the efficiency between our method and Gao's method [8]. Gao's approach is developed based on the classical 88-line 2D SIMP code [26] combining with the homogenization method. The same conditions are set as  $Lx = 10$ ,  $Ly = 5$ ,  $N_x^M = 100$ ,  $N_y^M = 50$ ,  $lx = 0.1$ ,  $ly = 0.1$ ,  $N_x^m = 50$ ,  $N_y^m = 50$ . The volume constraint  $V_0^M = 0.4$  and  $V^m = 0.6$  are taken. The initial shapes of macrostructure are  $\phi^M = V_0^M$ . The initial shapes of microstructure are Eq. (20). In our method, the parameters for macroscale are  $\eta^M = 2$ ,  $\beta^M = 2$ ,  $\gamma^M = 3$  and for microscale  $\eta^m = 0.01$ ,  $\beta^m = 0.5$ ,  $\gamma^m = 0.8$ . Other parameters are  $\epsilon^M = \epsilon^m = 0.01$  and  $\Delta t = 5h^M$ . Set  $\phi_{tol}^M = 0.01$  and  $\phi_{tol}^m = 0.01$  in both Gao's and our method. The optimized results obtained by multiscale topology optimization of Gao's method and our approach are shown in Table 4. It is clearly observed that the compliance  $\mathcal{J}$  obtained by our method is lower than Gao's method. We also compare the CPU time cost between Gao's method and our method. It takes 852.22s and 53.09s for Gao's method and our method, respectively. Besides, our method can remain the microstructure shape which may be beneficial to the manufacture in 3D prints. Therefore, it is concluded that our method is much faster and more efficient than Gao's method.

Comparison with one-scale topology optimization is also made. The problem (14) can naturally degrade to the one-scale optimization if we set one of the macro and micro volume as 1. For comparison, the total volume fraction is kept as above. When the micro volume fraction takes value of 1, only the macro topology is optimized. When the macro volume fraction equal to 1, only the micro topology is optimized with the effect of the macro loads and boundary conditions. The results are shown in Table. 4, the third and fourth rows respectively. We can see that for the cantilever beam the optimal result is

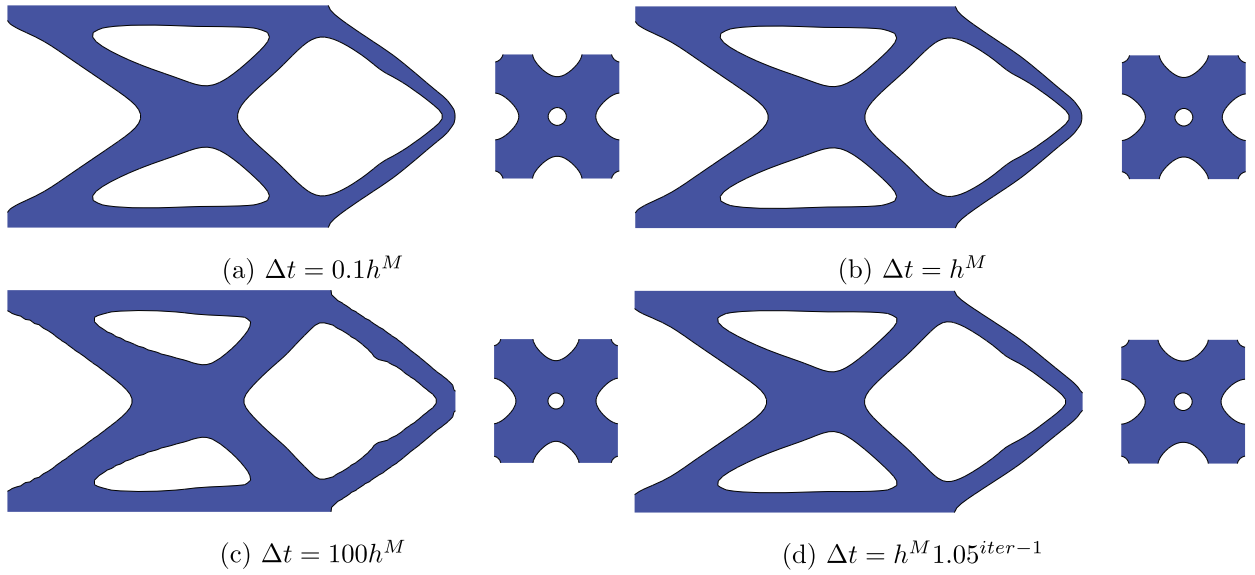


Fig. 5. The optimal design at time  $T = 300h^M$  with different time steps.

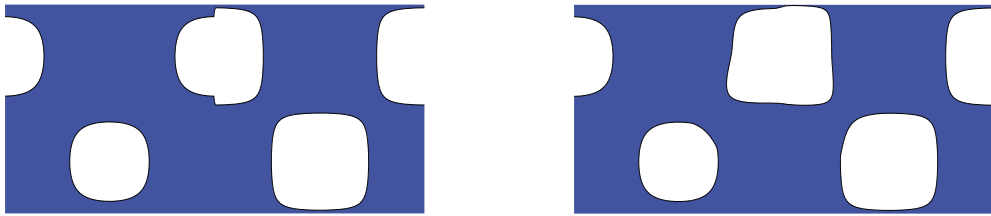


Fig. 6. Optimized microstructures with different porosities but similar shapes without and with connectivity constraints.

obtained by the single-scale topology optimization when micro fraction volume is equal to 1. The similar conclusions can be obtained in [8,18]. However, when more than one porous micro units in the macrostructure are optimized concurrently, the optimal design could have better performance than the single-scale topology optimization with micro volume fraction equal to 1. Assumed that there are five differently porous micro units in the macrostructure, the parameters are  $\eta^M = 1$ ,  $\beta^M = 2$ ,  $\gamma^M = 2$ , and micro-scale parameters for five different microstructures as  $\eta^m = (\eta_\tau^m) = [0.01; 0.01; 0.01; 0.01; 0.01]$ ,  $\beta^m = (\beta_\tau^m) = [0.5; 0.5; 0.5; 0.5; 0.5]$ ,  $\gamma^m = (\gamma_\tau^m) = [0.5; 0.5; 0.5; 0.5; 0.5]$ ,  $V^m = (V_\tau^m) = [0; 0.5; 0.6; 0.75; 1]$ ,  $\tau = 1, 2 \dots, 5$ . It is noted that  $V^m$  multiplying the areas of each subdomain is exactly equal to 0.6 which is same with the volume of one identical microstructure. The compliance of the optimal composite structure is  $\mathcal{J} = 95.11$  which performs better than the single-scale topology optimization  $\mathcal{J} = 108.46$  and the multiscale topology optimization of one identical microstructure in the macrostructure  $\mathcal{J} = 153.93$  shown in Table. 4. The details will be clarified in Section 6.4.

### 6.3. Connectivity test

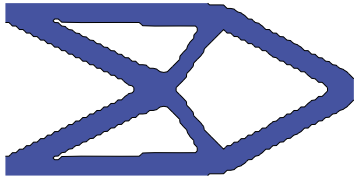

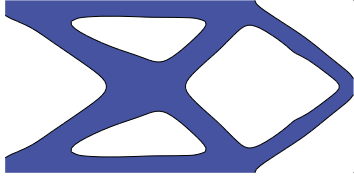

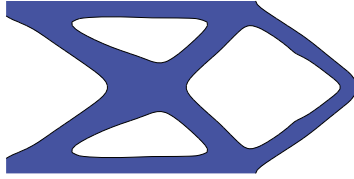



This test aims to investigate the connectivity of multiple microstructures using the merging algorithm and the modified AC type equation (18). We choose two adjacent cells which are connected incompletely (the left figure of Fig. 6) and two adjacent cells which are disconnected completely (the left figure of Fig. 7). By the interpolation technique and Eq. (18), the obtained structures are shown in the right figures of Fig. 6 and Fig. 7, respectively. As can be seen that the boundaries have been connected and the connected boundaries are smooth, which satisfies the theory of minimal surface.

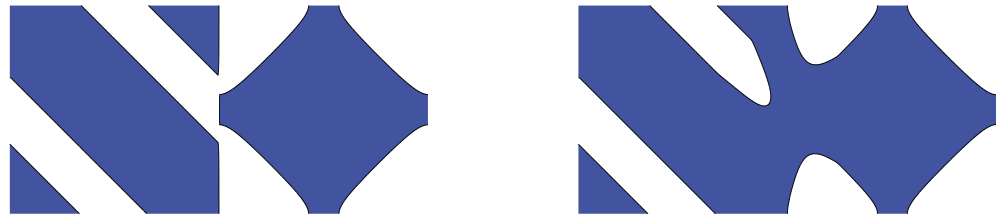
### 6.4. Concurrent optimization with multiple microstructures

In this test we consider concurrent topology optimization with five types of microstructures. In the stage of macrostructure topology optimization, according to the criteria in Table 1 mentioned before, the macro reference domain  $\Omega^M$  is approximately partitioned into five subdomains, represented by five different colors shown as in Fig. 8(a). And the obtained optimal topology shape of macrostructure is similar as Fig. 4(a) which is taken as the fixed macrostructure in next stage. In stage of the two-scale concurrent topology optimization, we set macro-scale parameters as  $\eta^M = 1$ ,  $\beta^M = 20$ ,  $\gamma^M = 100$ ,  $V_0^M = 0.4$  and micro-scale parameters for five different microstructures as  $\eta^m = (\eta_\tau^m) = [0.01; 0.1; 0.1; 0.1; 0.01]$ ,

**Table 4**

The optimal results by Gao's method [8] and the proposed method with the same initial shapes. From the upper to the bottom, the results are obtained by Gao's method, our method, single-scale topology optimization with the micro volume equal one, single-scale topology optimization with the macro volume equal one, respectively.

The optimized results of the cantilever beam		Homogenized elastic tensor	$\mathcal{J}$	CPU time
		$\begin{bmatrix} 0.5029 & 0.0908 & 0.0000 \\ 0.0908 & 0.1474 & 0.0000 \\ 0.0000 & 0.0000 & 0.1121 \end{bmatrix}$	201.60	852.22s
		$\begin{bmatrix} 0.6635 & 0.2344 & 0.0000 \\ 0.2344 & 0.6570 & 0.0000 \\ 0.0000 & 0.0000 & 0.2516 \end{bmatrix}$	148.80	53.09s
		$\begin{bmatrix} 1.0989 & 0.3297 & 0.0000 \\ 0.3297 & 1.0989 & 0.0000 \\ 0.0000 & 0.0000 & 0.3846 \end{bmatrix}$	108.46	35.15s
		$\begin{bmatrix} 0.2110 & 0.0635 & 0.0000 \\ 0.0635 & 0.2085 & 0.0000 \\ 0.0000 & 0.0000 & 0.0567 \end{bmatrix}$	218.67	36.54s



**Fig. 7.** Optimized microstructures with different shapes without and with connectivity constraints.

$\beta^m = (\beta_\tau^m) = [10; 20; 20; 20; 20]$ ,  $\gamma^m = (\gamma_\tau^m) = [100; 100; 100; 100; 100]$ ,  $V^m = (V_\tau^m) = [0; 0.4; 0.6; 0.8; 1]$ ,  $\tau = 1, 2 \dots, 5$ . Assume that the macro initial topology shape in stage 2 is set as  $\phi_0^M = V_0^M$  and the micro initial ones are same with the prescribed ones with periodic minimal surfaces. Let  $\psi^M$  represent the fixed macro topology shapes shown in Fig. 4(a). Let  $\psi_\tau^m$  ( $\tau = 1, 2, \dots, 5$ ) represent the prescribed microstructures shown in Table 5 'Initial micro'. Table 5 shows the details about the optimal topologies of microstructures in the concurrent optimization. We can observe that the obtained optimal topologies of the microstructures are nearly same with the initial ones. Fig. 8(b) shows the optimal topologies of the composite structure obtained by our systematic multi-scale concurrent topology optimization method.

Fig. 9 shows the connected boundaries between two different cells by the interpolation mechanism. But this interpolation mechanism might damage the optimized performance. We provide the comparisons of the compliance problem and the micro homogenized elastic tensors to present the difference of procedures before and after the connectivity technique. For this case in Fig. 8(b), the compliance of macrostructure increase 17% after the connectivity procedure. We display the micro homogenized elastic tensors of the elements near the blue solid line as shown in Fig. 8(b). Because of the cantilever beam's symmetry, we only show the micro homogenized elastic tensors at the top half marked solid line in Table 6. It is obvious that the micro homogenized elastic tensor at the connected boundary after the connecting technique asymptotically approaches those before the connectivity technique.

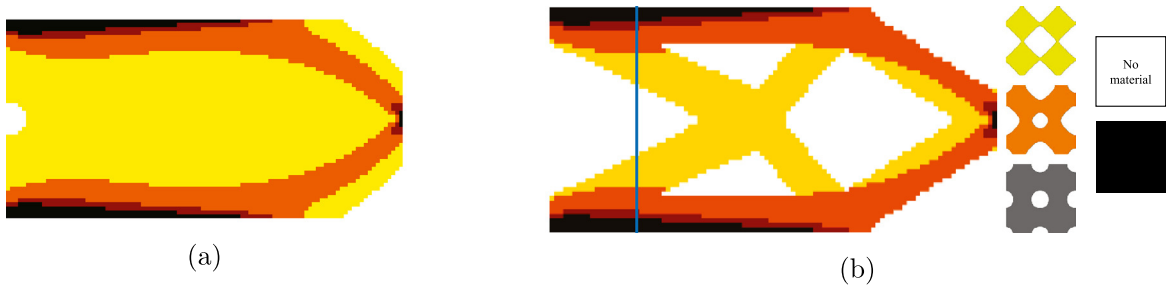


Fig. 8. (a) The regularized domain; (b) the optimal composite macrostructure; the blue solid line is used to make a mark of the one fifth as long.

Table 5

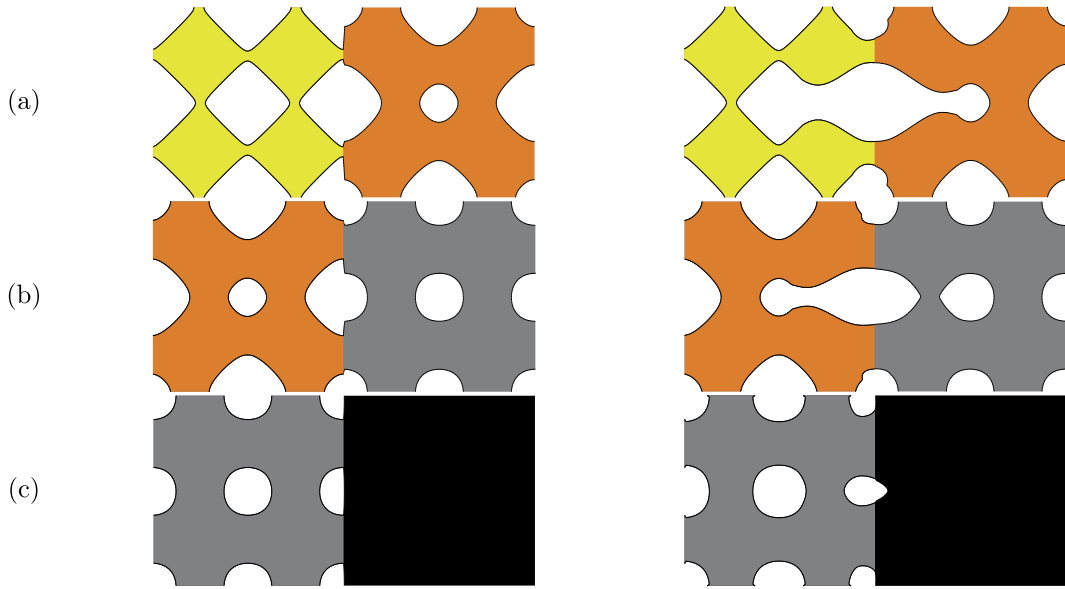
The optimized results by our concurrent topology optimization with multiple microstructures.  $Vol_0$  and  $Vol_1$  represent the volume fraction of initials shapes and optimized shapes for multiple microstructures.

No.	$Vol_0$	$Vol_1$	Initial micro	Optimized micro	Homogenized elastic tensor
2	50%	46%			$\begin{bmatrix} 0.0834 & 0.0072 & 0.0000 \\ 0.0072 & 0.0827 & 0.0000 \\ 0.0000 & 0.0000 & 0.0145 \end{bmatrix}$
3	60%	58%			$\begin{bmatrix} 0.1763 & 0.0490 & 0.0000 \\ 0.0490 & 0.1755 & 0.0000 \\ 0.0000 & 0.0000 & 0.0506 \end{bmatrix}$
4	75%	76%			$\begin{bmatrix} 0.4650 & 0.0957 & 0.0000 \\ 0.0957 & 0.4642 & 0.0000 \\ 0.0000 & 0.0000 & 0.1101 \end{bmatrix}$
5	100%	100%			$\begin{bmatrix} 1.0980 & 0.3293 & 0.0000 \\ 0.3293 & 1.0980 & 0.0000 \\ 0.0000 & 0.0000 & 0.3842 \end{bmatrix}$

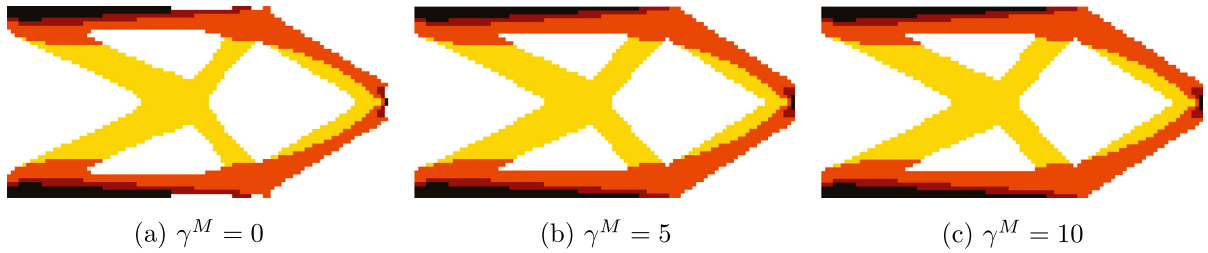
Table 6

The micro homogenized elastic tensors of 25 macro elements near the upper half part of the blue solid line (from top to bottom). Num. 18 - Num. 25 have been omitted, because no materials appear in these regions.

Num.	1 – 2	3	4
Tensor	$\begin{bmatrix} 1.0980 & 0.3293 & 0.0000 \\ 0.3293 & 1.0980 & 0.0000 \\ 0.0000 & 0.0000 & 0.3842 \end{bmatrix}$	$\begin{bmatrix} 0.8412 & 0.2505 & 0.0000 \\ 0.2505 & 0.9683 & 0.0000 \\ 0.0000 & 0.0000 & 0.3083 \end{bmatrix}$	$\begin{bmatrix} 0.2556 & 0.0550 & 0.0000 \\ 0.0550 & 0.3988 & 0.0000 \\ 0.0000 & 0.0000 & 0.0657 \end{bmatrix}$
Num.	5	6	7 – 9
Tensor	$\begin{bmatrix} 0.3203 & 0.0563 & 0.0150 \\ 0.0563 & 0.3219 & 0.0147 \\ 0.0150 & 0.0147 & 0.0699 \end{bmatrix}$	$\begin{bmatrix} 0.1225 & 0.0389 & 0.0000 \\ 0.0389 & 0.1613 & 0.0000 \\ 0.0000 & 0.0000 & 0.0390 \end{bmatrix}$	$\begin{bmatrix} 0.1763 & 0.0490 & 0.0000 \\ 0.0490 & 0.1755 & 0.0000 \\ 0.0000 & 0.0000 & 0.0506 \end{bmatrix}$
Num.	10	11	12 – 17
Tensor	$\begin{bmatrix} 0.1292 & 0.0419 & 0.0011 \\ 0.0419 & 0.1891 & 0.0012 \\ 0.0011 & 0.0012 & 0.0429 \end{bmatrix}$	$\begin{bmatrix} 0.0453 & 0.0043 & 0.0000 \\ 0.0043 & 0.0594 & 0.0000 \\ 0.0000 & 0.0000 & 0.0083 \end{bmatrix}$	$\begin{bmatrix} 0.0834 & 0.0072 & 0.0000 \\ 0.0072 & 0.0827 & 0.0000 \\ 0.0000 & 0.0000 & 0.0145 \end{bmatrix}$



**Fig. 9.** Schematic of the connectivity between multiple micro structures in our concurrent optimization. The left column is obtained without connectivity constraints and the right column is obtained with connectivity constraints. (a), (b) and (c) depict the connectivity between cells in Table 5 of No.2 and No.3, No.3 and No.4, No.4 and No.5, respectively.



**Fig. 10.** The optimal topology shapes of the macrostructures with different values of  $\gamma^M=0, 5, 10$ . Correspondingly, the number of iterations are 50, 30, 17 and the objective are 675.10, 913.44, 967.54, respectively.

6.5. Effect of the parameter  $\gamma$

In Eqs. (16)-(17),  $\gamma$  plays an important role to keep the optimal shapes as closed as the fixed shapes both for macro-scale and micro-scale. This test aims to verify  $\gamma^M$  and  $\gamma_\tau^m$  indeed have effect on maintaining the topology shapes of macro-scale and micro-scale. In stage 1, the fixed macrostructure is same as Fig. 4(a). In stage 2, we take the parameters as  $\eta^M = 1, \beta^M = 20, \eta_\tau^m = [0.01; 0.1; 0.1; 0.1; 0.01], \beta_\tau^m = [10; 20; 20; 20; 10], \gamma_\tau^m = [10; 10; 10; 10; 10]$ . We firstly perform the concurrent topology optimization with  $\gamma^M = 0, 5, 10$ , while other parameters keep unchanged. The initial shapes are assumed as same as Section 6.4. The optimal shapes of macrostructure are obtained as shown in Fig. 10, from which we observe that the final topology shape has a rougher surface with  $\gamma^M = 0$  than with  $\gamma^M = 5, 10$ . The number of iterations are 50, 30, 17 correspondingly to  $\gamma^M = 0, 5, 10$ , and the objectives  $\mathcal{J} = 675.10, 913.44, 967.54$  respectively.

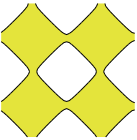
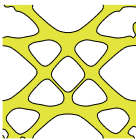
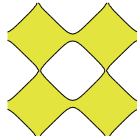
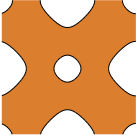
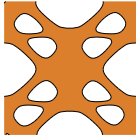
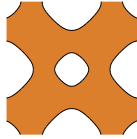
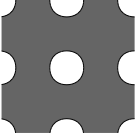
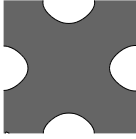
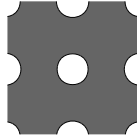
Next we perform concurrent topology optimization with different values of  $\gamma_\tau^m = [10; 0; 0; 0; 10]$  and  $[10; 10; 10; 10; 10]$  ( $\tau = 1, 2, \dots, 5$ ) with  $\gamma^M = 5$  while other parameters keep unchanged. The first and last microstructures always keep as same as what they should be thus we do not consider them. For the other micro-cells, the results in Table 7 indicate that when  $\gamma_\tau^m$  takes value of 0, there is a phenomenon of nucleation for the microstructure whose volume fraction decreases. As the values of  $\gamma_\tau^m$  increase, the shapes become as much as closed to the initial shapes which verifies that  $\gamma_\tau^m$  indeed maintain the optimized shape same with the initial shape of microstructure.

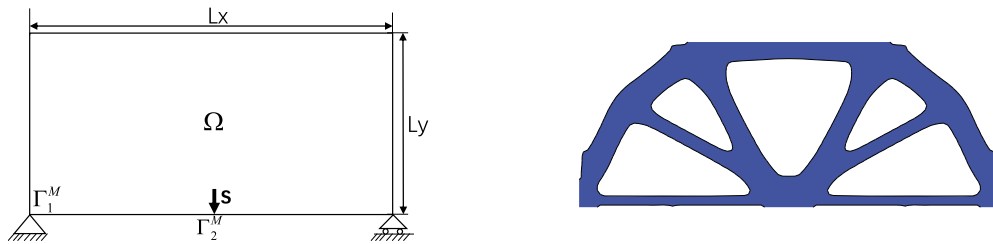
6.6. Effect of the parameter  $\beta$

This experiment takes an example of the classical Michell-type structure. The size parameters are set as  $Lx = 10, Ly = 4, N_x^M = 100, N_y^M = 40, lx = 0.1, ly = 0.1, N_x^m = 50, N_y^m = 50$ . The left bottom and the right bottom are supported and a traction force  $\mathbf{s} = -1$  is loaded on the middle point of the bottom side. In stage 1, we set  $V_0^M = 0.4$ , and the initial shape of macrostructure is set as  $\phi_0^M = V_0^M$ . The other parameters are set as  $\eta^M = 10, \beta = 20, \gamma^M = 0$ . The schematic of

**Table 7**

The optimal micro shapes with  $\gamma_\tau^m = 0, 10$ . Here  $V_0, V_1$  and  $V_2$  represent the volume fractions of the initial micro shapes, the optimal micro shape 1 with  $\gamma_\tau^m = 0$  and the optimal micro shape 2 with  $\gamma_\tau^m = 10$  respectively. Besides, the objectives are  $J^* = 729.14$  and  $913.44$ .

No.	Initial shapes	$V_0$	Optimal shapes 1	$V_1$	Optimal shapes 2	$V_2$
2		50%		32%		36%
3		60%		51%		53%
4		75%		80%		80%



**Fig. 11.** From left to right, they are the schematic of classical Michell-type structure and the fixed macrostructure obtained in stage 1 respectively.

classical Michell-type structure and the fixed macrostructure obtained in stage 1 are shown in Fig. 11. Next, we consider the effect of  $\beta^M$  on the volumes of macrostructure and microstructures in stage 2. In this text, the type of micro unit cell is D-surface, i.e.  $(\phi_\tau^m)^0(x, y) = 0.5(1 - \cos 2\pi x \cos 2\pi y + \sin 2\pi x \sin 2\pi y)$ . Assuming that the design domain is partitioned into five subdomains, the initial microstructures are shown in Fig. 14(a), where no material cell and full solid cell are not depicted. For simplicity, the volume fractions of these three microstructures are chosen as 0.5. The initial macro volume fraction (same with the volume fraction of the fixed Michell-type structure) in stage 2 is 0.47 which is different from the volume fraction constraint  $V_0^M = 0.4$ . We perform multi-scale concurrent topology optimization with different values of  $\beta^M = 0, 10, 100, 1000$ . Other parameters are set as  $\eta_\tau^m = 1, \gamma_\tau^m = 10(\tau = 1, 2, \dots, 5), \eta^M = 5, \beta^M = 20, \gamma^M = 10, \Delta t = 0.001$  and  $T = 30$ . Fig. 12 and Fig. 13 display the obtained optimal macrostructures and the curves of volume evolution for the macrostructure with  $\beta^M = 0, 10, 100, 1000$ , from which we can see that larger  $\beta^M$  can make the volume fraction of the optimal structure as much as close to  $V_0^M = 0.4$ . And the effect of  $\beta^M$  on the micro-scale cell can be neglected and the final topologies of micro cells with  $\beta^M = 0, 10, 100, 1000$  are similar as shown in Fig. 14(c).

Next we consider the effect of  $\beta_\tau^m$  on the topologies of microstructures and macrostructure. We keep the initial shapes of microstructures as Fig. 14(a). Fig. 14(b)-(d) are the obtained results using different values of  $\beta_\tau^m$ . It's indicated that different  $\beta_\tau^m$  has an effect on the convergence of the volume fraction of microstructure. The initial volume fractions of the three microstructures are set as [0.50; 0.50; 0.50] and the prescribed volume fractions we set as [0.6; 0.6; 0.6]. When  $\beta_\tau^m = 0$ , the volume fraction of the three microstructures is [0.55; 0.57; 0.61]. And when  $\beta_\tau^m = 2$ , the volume fractions of the three microstructures become [0.60; 0.61; 0.60] which are close to the prescribed volume fractions. The effect of  $\beta_\tau^m$  on the topology of macrostructure can be neglected, thus not specified here.

6.7. Effect of the parameter  $\eta$

We use the classical MBB structure to study the effect of  $\eta$  in Eq. (8). In order to verify that the proposed method can be used with other minimal surface units, we use G-surface unit cells as the microstructures in this test. The schematic diagram of MBB is shown in Fig. 15. Here  $Lx = 15, Ly = 3, N_x^M = 150, N_y^M = 30, l_x = 0.1, l_y = 0.1, N_x^m = 50, N_y^m = 50$ . The bottom side is fixed and a traction force  $s = -1$  is loaded on the middle point of the top side. In stage 1, the parameters



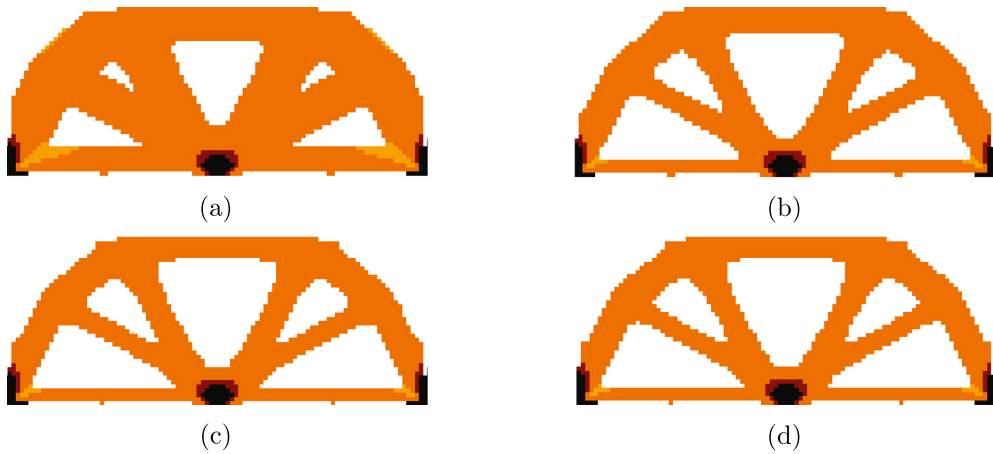


Fig. 12. The optimized Michell-type structures (a)-(d) corresponding to  $\beta^M = 0$ ,  $\beta^M = 10$ ,  $\beta^M = 100$ ,  $\beta^M = 1000$ , respectively.

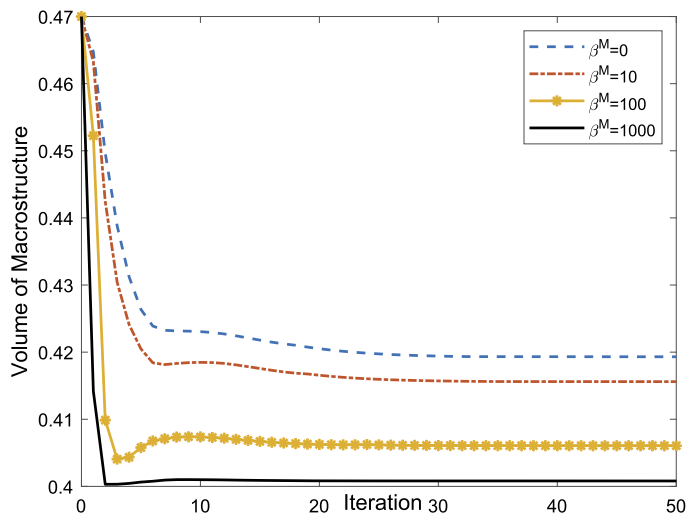


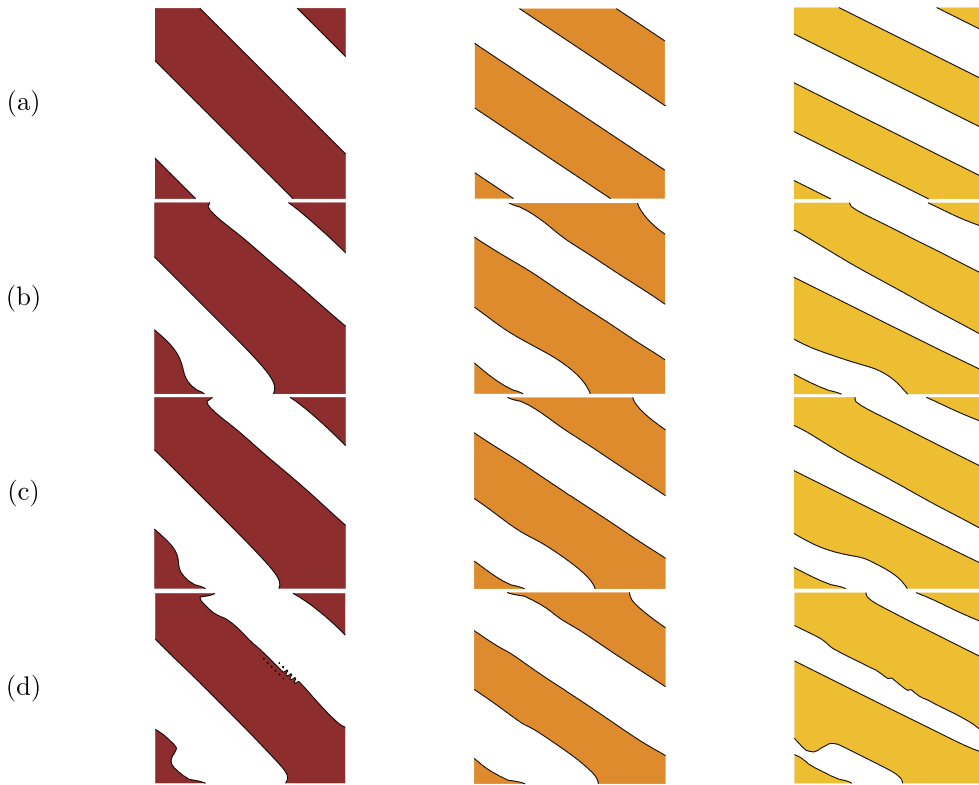
Fig. 13. Comparison of the macrostructural volume evolution between different values of  $\beta^M$ .

we set are  $\beta^M = 100$ ,  $\eta^M = 6$ ,  $\gamma^M = 0$ ,  $V_0^M = 0.4$  and  $\phi_0^M = V_0^M$ . We obtain the optimal macrostructure by macro topology optimization shown in Fig. 15, which is similar design as other previous works [8]. Then we take this optimal result as the fixed macro shape in stage 2. In stage 2, i.e. multiscale concurrent topology optimization, let  $\gamma^M = 10$ ,  $\eta^M = 5$ ,  $\beta_\tau^M = 100$ ,  $\gamma_\tau^m = 10$ ,  $\eta_\tau^m = 1$ ,  $\beta_\tau^m = 2$ ,  $T = 0.02$ ,  $\Delta t = 0.001$ . The results are shown as follows. The subregions shown in Fig. 16(a) are partitioned according to Table. 4. Fig. 16(b) displays the optimal macro- and microstructures obtained by the proposed method. Here, the void and fully solid units have been omitted for simplicity. The connectivity between two microstructures is shown in Fig. 17.

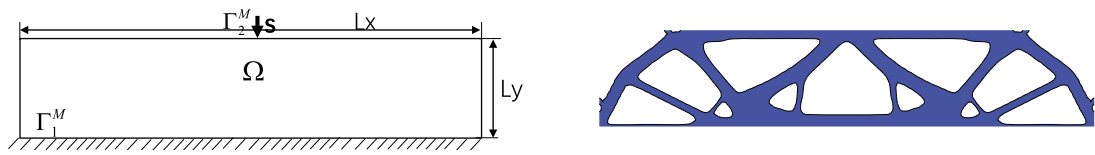
Next, we are going to study the effect of  $\eta$  in Eq. (8). By changing the values of  $\eta^M$ , we obtain these results displayed in Fig. 18. The compliance  $\mathcal{J}$  of MBB decreases as the values of  $\eta^M$  increase, meanwhile the size of holes in MBB structures increases. Then we change the values of  $\eta_\tau^m = 0, 1, 5$  while keep  $\eta^M = 10$  and other parameters fixed to study the effect of  $\eta_\tau^m$  on the microstructures and objective. Fig. 19 shows us that  $\eta_\tau^m$  insignificantly affects the topologies of microstructures but significantly affects the size of micro shapes. The larger values of  $\eta_\tau^m$  can lead to small size holes in the microstructures. The compliances of MBB are  $\mathcal{J} = 484.6, 309.4$ , and  $186.5$  respectively, which indicates the value of  $\eta_\tau^m$  has the similar influence on the MBB compliance.

### 7. Conclusion

An efficient and systematic PFM-based multiscale topology optimization method was proposed. This method not only optimized the composite structure but also solved the problem of connectivity between different types of microstructures. The modified Allen-Cahn type equations based on phase field method were used to evolve the macro and micro design variables. And second-order accurate numerical schemes for the evolved equations based on Adam’s time discretization



**Fig. 14.** The initial microstructures (a) for Michell-type structure, no material cell and full solid cell are not specified here. (b)-(d) are the optimal topology of multiple microstructures, which corresponds to  $\beta_r^m = [0; 0; 0], [2; 2; 2], [20; 20; 20]$ , respectively.  $\beta^M = 100$ .

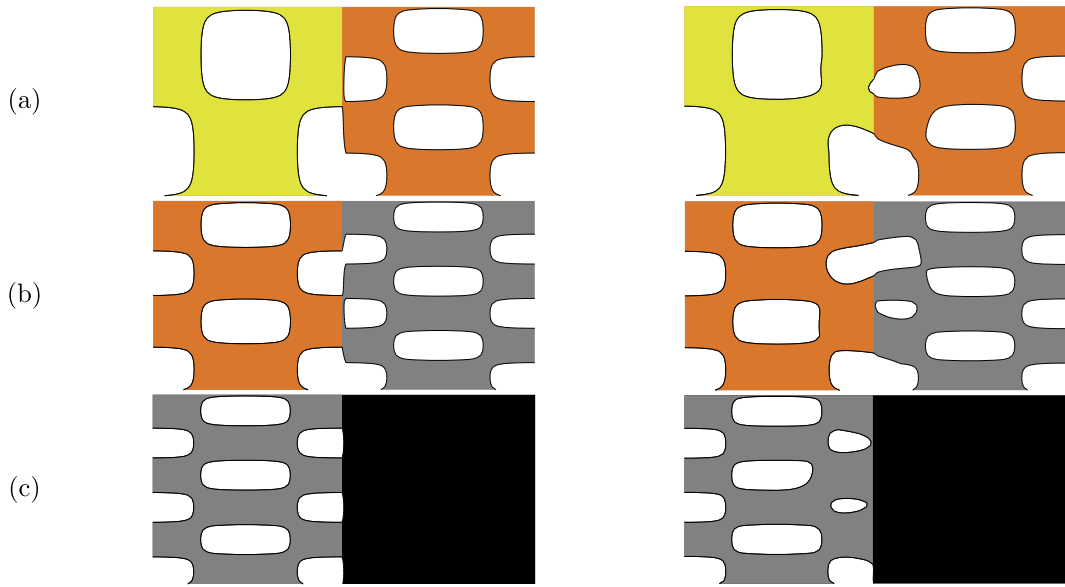


**Fig. 15.** The schematic diagram of MBB structure and the optimal design obtained in stage 1.

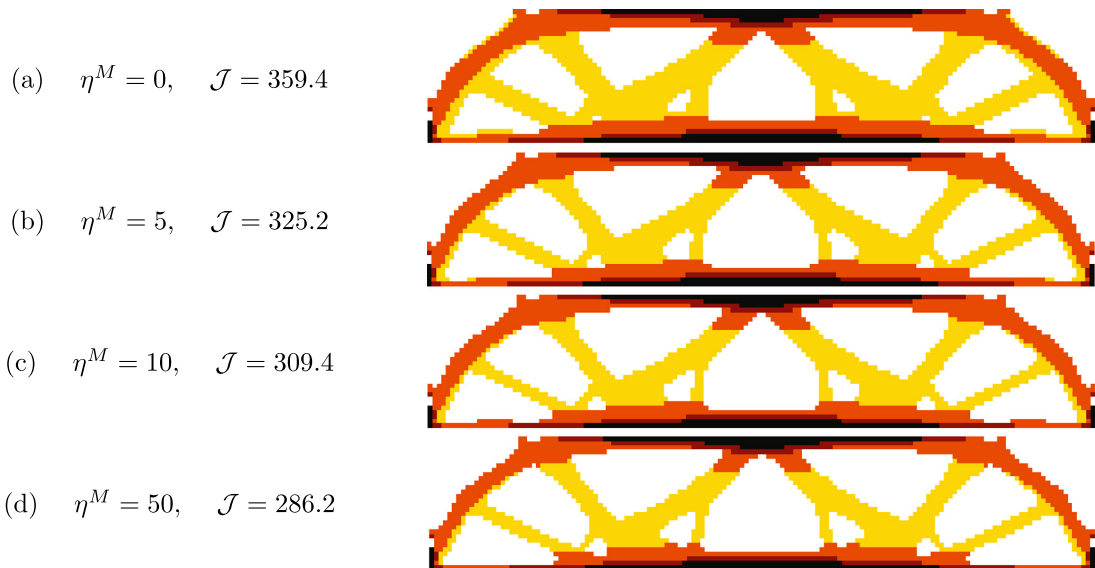


**Fig. 16.** The regularized design region for MBB structure and the optimal results obtained by the proposed method.

method were proposed. The boundaries between different microstructures connected by our method were smooth and satisfied the minimal surface theorem which improved the stability of the composite structure. The implementation of PFM-based topology optimization was very simple. The proposed method overcame the difficulty of indeterminate pores of materials in the homogenization method and performed better in computation efficiency and stability than SIMP [8]. In the process of optimization, our method did not require the re-initialization or the velocity extension which were required in LSM (Hamilton-Jacobi based). A large time step was allowed in our scheme so there would be no need of a large number of iterations in the optimization. Just like phase transition, nucleating new holes inside the material domain was also allowed. By numerical simulations, we obtained that the optimal design by our method with multiple microstructures had better performance than by the single-scale topology optimization. And our method with one identical microstructure had a better stiffness performance than Gao's [8] in which the modified SIMP was used. As for the sensitivity analysis of parameters in the evolved equations, we obtained that the coefficients before the correction terms could keep the topology shapes as same



**Fig. 17.** Schematic of the connectivity between G-surface microstructures in the design of MBB. The left column is obtained without connectivity constraints and the right column is obtained with connectivity constraints.

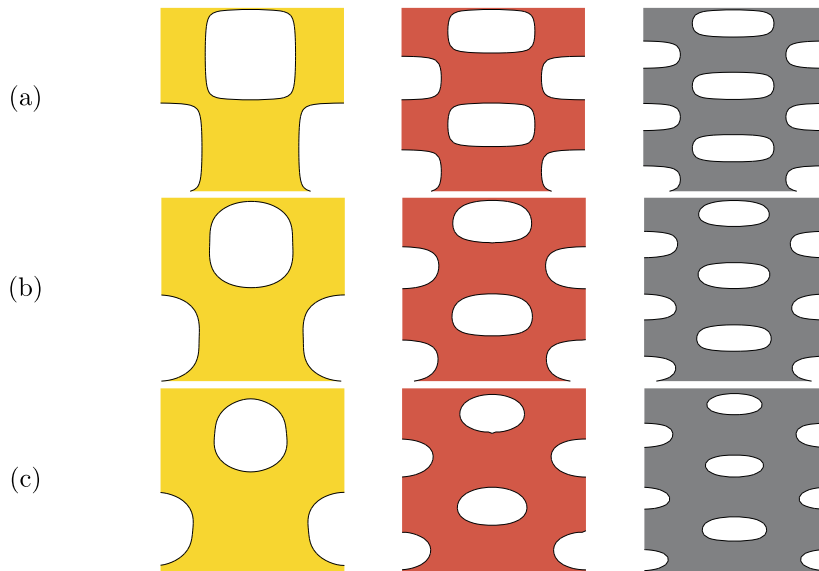


**Fig. 18.** The optimized MBB structures with different values of  $\eta^M$ .  $\mathcal{J}$  is the compliance corresponding to  $\eta^M = 0, 5, 10, 50$ , respectively.

as the fixed. The coefficients before the volume constraint terms could make the volume fractions closed to the maximum volume fractions. The coefficients before the topology sensitivity term could affect the optimal topology shapes. Noted that in real manufacture, we should choose appropriate coefficients to meet different requirements. In the future, the adaptively updated coefficients will be considered to improve the performance of the proposed algorithm.

**CRedit authorship contribution statement**

**Qian Yu:** Conceptualization, Investigation, Methodology, Software, Visualization, Writing – original draft. **Qing Xia:** Conceptualization, Supervision, Writing – review & editing. **Yibao Li:** Conceptualization, Methodology, Project administration, Software, Supervision, Writing – review & editing.



**Fig. 19.** (a)-(c): the optimal topologies of multiple microstructures, which correspond to  $\eta_c^m = [0; 0; 0]$ ,  $[1; 1; 1]$ ,  $[5; 5; 5]$ , respectively, with  $\eta^M = 10$  fixed. The void cell and full solid cell are not specified here.

### Declaration of competing interest

The authors declare that they have no known competing financial interests or personal relationships that could have appeared to influence the work reported in this paper.

### Acknowledgement

This work is supported by the Fundamental Research Funds for the Central Universities (No. XTR042019005). The authors also thank the reviewers for the constructive and helpful comments on the revision of this article.

### References

- [1] L.J. Gibson, M.F. Ashby, *Cellular Solids: Structure and Properties*, Cambridge University Press, 1999.
- [2] Y. Zheng, Z. Luo, Y. Wang, Z. Li, J. Qu, C. Zhang, Optimized high thermal insulation by the topological design of hierarchical structures, *Int. J. Heat Mass Transf.* 186 (2022) 122448.
- [3] F. Weina, N. Chen, N. Iqbal, M. Stingl, M. Avila, Topology optimization of unsaturated flows in multi-material porous media: application to a simple diaper model, *Commun. Nonlinear Sci. Numer. Simul.* 78 (2019) 104871.
- [4] S.C. Han, J.W. Lee, K. Kang, A new type of low density material: Shellular, *Adv. Mater.* 27 (2015) 5506–5511.
- [5] H. Li, Z. Luo, L. Gao, Q. Qin, Topology optimization for concurrent design of structures with multi-patch microstructures by level sets, *Comput. Methods Appl. Mech. Eng.* 331 (2018) 536–561.
- [6] J. Gao, Z. Luo, H. Li, L. Gao, Topology optimization for multiscale design of porous composites with multi-domain microstructures, *Comput. Methods Appl. Mech. Eng.* 344 (2019) 451–476.
- [7] J. Gao, Z. Luo, H. Li, P. Li, L. Gao, Dynamic multiscale topology optimization for multi-regional microstructured cellular composites, *Compos. Struct.* 211 (2019) 401–417.
- [8] J. Gao, Z. Luo, L. Xia, L. Gao, Concurrent topology optimization of multiscale composite structures in Matlab, *Struct. Multidiscip. Optim.* 60 (2019) 2621–2651.
- [9] D. Da, X. Cui, K. Long, Y. Cai, G. Li, Multiscale concurrent topology optimization of structures and microscopic multi-phase materials for thermal conductivity, *Eng. Comput.* 36 (1) (2019) 126–146.
- [10] D. Kim, J. Lee, T. Nomurab, E.M. Dedec, J. Yood, S. Mine, Topology optimization of functionally graded anisotropic composite structures using homogenization design method, *Comput. Methods Appl. Mech. Eng.* 369 (2020) 113220.
- [11] T. Kumar, S. Sridhara, B. Prabhune, K. Suresh, Spectral decomposition for graded multi-scale topology optimization, *Comput. Methods Appl. Mech. Eng.* 377 (2021) 113670.
- [12] K. Long, D. Han, X. Gu, Concurrent topology optimization of composite macrostructure and microstructure constructed by constituent phases of distinct Poisson's ratios for maximum frequency, *Comput. Mater. Sci.* 129 (2017) 194–201.
- [13] Y. Zhang, M. Xiao, L. Gao, J. Gao, H. Li, Multiscale topology optimization for minimizing frequency responses of cellular composites with connectable graded microstructures, *Mech. Syst. Signal Process.* 135 (2020) 106369.
- [14] O. Sigmund, K. Maute, Topology optimization approaches: a comparative review, *Struct. Multidiscip. Optim.* 48 (2013) 1031–1055.
- [15] J. Wu, O. Sigmund, J.P. Groen, Topology optimization of multi-scale structures: a review, *Struct. Multidiscip. Optim.* 63 (2021) 1455–1480.
- [16] H. Li, Z. Luo, N. Zhang, L. Gao, T. Brown, Integrated design of cellular composites using a level-set topology optimization method, *Comput. Methods Appl. Mech. Eng.* 309 (2016) 453–475.
- [17] R. Sivapuram, P.D. Dunning, H.A. Kim, Simultaneous material and structural optimization by multiscale topology optimization, *Struct. Multidiscip. Optim.* 54 (2016) 1267–1281.

- [18] Y. Wang, Z. Kang, Concurrent two-scale topological design of multiple unit cells and structure using combined velocity field level set and density model, *Comput. Methods Appl. Mech. Eng.* 347 (2019) 340–364.
- [19] S. Zhou, Q. Li, Design of graded two-phase microstructures for tailored elasticity gradients, *J. Mater. Sci.* 43 (2008) 5157–5167.
- [20] Z. Du, X. Zhou, R. Picelli, H.A. Kim, Connecting microstructures for multiscale topology optimization with connectivity index constraints, *J. Mech. Des.* 140 (2018) 111417.
- [21] M.P. Bendsøe, O. Sigmund, *Topology Optimization: Theory, Methods, and Applications*, Springer Science & Business Media, 2003.
- [22] M.P. Bendsøe, N. Kikuchi, Generating optimal topologies in structural design using a homogenization method, *Comput. Methods Appl. Mech. Eng.* 71 (1988) 197–224.
- [23] J.M. Guedes, N. Kikuchi, Preprocessing and postprocessing for materials based on the homogenization method with adaptive finite element methods, *Comput. Methods Appl. Mech. Eng.* 83 (1990) 143–198.
- [24] G. Allaire, L. Cavallina, N. Miyake, T. Oka, T. Yachimura, The homogenization method for topology optimization of structures: old and new, *Interdiscip. Inf. Sci.* 25 (2) (2019) 75–146.
- [25] M. Zhou, G.I.N. Rozvany, The COC algorithm, part II: topological, geometrical and generalized shape optimization, *Comput. Methods Appl. Mech. Eng.* 89 (1991) 309–336.
- [26] E. Andreassen, A. Clausen, M. Schevenels, B.S. Lazarov, O. Sigmund, Efficient topology optimization in Matlab using 88 lines of code, *Struct. Multidiscip. Optim.* 43 (2011) 1–16.
- [27] Y.M. Xie, G.P. Steven, A simple evolutionary procedure for structural optimization, *Comput. Struct.* 49 (5) (1993) 885–896.
- [28] X. Huang, S. Zhou, Y. Xie, Q. Li, Topology optimization of microstructures of cellular materials and composites for macrostructures, *Comput. Mater. Sci.* 67 (2013) 397–407.
- [29] M.Y. Wang, X. Wang, D. Guo, A level set method for structural topology optimization, *Comput. Methods Appl. Mech. Eng.* 192 (2003) 227–246.
- [30] Z. Luo, M.Y. Wang, S. Wang, P. Wei, A level set-based parameterization method for structural shape and topology optimization, *Int. J. Numer. Methods Eng.* 76 (2008) 1–26.
- [31] J. Zhao, X. Yang, Y. Gong, X. Zhao, X. Yang, J. Li, Q. Wang, A general strategy for numerical approximations of non-equilibrium models-part 1: thermodynamical systems, *Int. J. Numer. Anal. Model.* 15 (6) (2018) 884–918.
- [32] X. Meng, Z. Qiao, C. Wang, Z. Zhang, Artificial regularization parameter analysis for the no-slope-selection epitaxial thin film model, *SIAM T. Appl. Math.* 1 (2020) 441–462.
- [33] Y. Gong, J. Zhao, Q. Wang, Arbitrarily high-order linear energy stable schemes for gradient flow models, *J. Comput. Phys.* 419 (2020) 109610.
- [34] Y. Li, K. Wang, Q. Yu, Q. Xia, J. Kim, Unconditionally energy stable schemes for fluid-based topology optimization, *Commun. Nonlinear Sci. Numer. Simul.* 111 (2022) 106433.
- [35] A. Takezawa, S. Nishiwaki, M. Kitamura, Shape and topology optimization based on the phase field method and sensitivity analysis, *J. Comput. Phys.* 229 (2010) 2697–2718.
- [36] J.S. Choi, T. Yamada, K. Izui, S. Nishiwaki, J. Yoo, Topology optimization using a reaction-diffusion equation, *Comput. Methods Appl. Mech. Eng.* 200 (2011) 2407–2420.
- [37] S.M. Allen, J.W. Cahn, A microscopic theory for antiphase boundary motion and its application to antiphase domain coarsening, *Acta Metall.* 27 (6) (1979) 1085–1095.
- [38] Y. Li, S. Guo, Triply periodic minimal surface using a modified Allen-Cahn equation, *Appl. Math. Comput.* 295 (2017) 84–94.
- [39] M. Carraturo, E. Rocca, E. Bonetti, D. Hömberg, A. Reali, F. Auricchio, Graded-material design based on phase-field and topology optimization, *Comput. Mech.* 64 (2019) 1589–1600.
- [40] F. Auricchio, E. Bonetti, M. Carraturo, D. Hömberg, A. Reali, E. Rocca, A phase-field-based graded-material topology optimization with stress constraint, *Math. Models Methods Appl. Sci.* 30 (8) (2020) 1461–1483.
- [41] Q. Yu, K. Wang, B. Xia, Y. Li, First and second order unconditionally energy stable schemes for topology optimization based on phase field method, *Appl. Math. Comput.* 405 (2021) 126267.
- [42] H. Chi, Y. Zhang, T. Tang, L. Mirabella, L. Dalloro, L. Song, G.H. Paulino, Universal machine learning for topology optimization, *Comput. Methods Appl. Mech. Eng.* 375 (2021) 112739.
- [43] Y. Li, Q. Xia, S. Yoon, C. Lee, B. Lu, J. Kim, Simple and efficient volume merging method for triply periodic minimal structures, *Comput. Phys. Commun.* 264 (2021) 107956.